UNIVERSITY OF CANTERBURY

Department of Physics and Astronomy

CHRISTCHURCH NEW ZEALAND

General Relativistic Galaxy Models

Cathy NEILL

MAPH480 PROJECT REPORT 2011

Supervisors: Assoc. Prof. David L. WILTSHIRE,
Dr. Teppo MATTSSON

Abstract

In 2006 Cooperstock and Tieu suggested that the spherical dark matter halos used to successfully model the rotation curves of spiral galaxies with Newtonian dynamics are not required. Instead, one can use rotating dust solutions purely in general relativity. This work is controversial and various technical points are disputed. The follow-up paper by Balasin and Grumiller, which comes to similar conclusions, also has some technical flaws. In this project we investigate, with a view to potentially improve, these results.

We find that Cooperstock and Tieu's model does not give physically reasonable behaviour at spatial infinity in the radial direction. Additionally, we find that the particular solution of Cooperstock and Tieu is not consistent with a prescribed empirical density profile, even though we show that the general system of equations is. We also find that the boundary conditions imposed to obtain Balasin and Grumiller's solution are unsuitable, as these were set in regions which are not physically admissible. Moreover, we discover contradictions arising from the separation ansatz used in both papers, suggesting that one must instead solve the system of equations more generally, with care taken to set physically reasonable boundary conditions. Towards this end we have obtained a first order partial differential equation from the system of equations which may be solved in future work.

While the general relativistic approach may not eliminate the need for nonbaryonic dark matter, it might produce a different value of the dark matter-to-baryon ratio which may be significant in discriminating between different cosmological models.

Contents

Chapter 1

Introduction

1.1 The History of Dark Matter Theories

The idea that luminous matter could only account for a small amount of all the matter in the Universe was introduced by Fritz Zwicky in 1934. From his observations of the rotation velocities of galaxies in the Coma cluster he inferred that there should be 400 times more mass than was observed (though with a more modern figure for the Hubble constant, this would be reduced to 50) [1]. This was because the gravitational attraction of the observable matter would be too small to hold the cluster together given the speed of orbits observed. Though it was Zwicky who first coined the term "dunkle kalte Materie" ("Dark cold matter"), it was not used in the same sense as the modern use of the term. Hypotheses of the time focussed on hidden heavy objects made of ordinary matter as possible causes of the mass discrepancy. These days we would class these as neutron stars, faint old white dwarfs and brown dwarfs. However, not enough of these objects, collectively known as Massive astrophysical compact halo objects ("MACHOS"), have been observed to account for the extra mass [2, 3, 4].

Nowadays it is believed that the majority of dark matter is nonbaryonic, not comprised of atoms. There exist three main hypothesised types of nonbaryonic dark matter [5]:

- Cold Dark Matter (CDM): particles that move non-relativistically
- Warm dark matter (WDM): particles that move relativistically
- Hot dark matter (HDM): particles that move ultra-relativistically (speeds >99% of speed of light, commonly neutrinos)

As more massive objects move more slowly on average, hypotheses involving cold dark matter are better able to explain that a large fraction of the mass of the universe appears to be non-luminous matter. There are models that attempt to explain the galaxy rotation speed problem without cold dark matter by modification of the laws of gravitation used, such as the purely phenomenological Modified Newtonian dynamics (MOND) model. The present standard model of cosmology, ΛCDM (Lambda Cold Dark Matter) incorporates both CDM and a cosmological constant.

Attempts to directly observe any forms of dark matter that could account for the observations of Zwicky and many others have so far not had any conclusive success. although there are some claimed detections [6] which are much debated. There are several key observational indications of its existence, however. Importantly, these all involve the effects of dark matter via gravity alone. The most important pieces of evidence are:

- Gravitational lensing due to massive objects gravitationally deflecting light. By measuring the distortion geometry, the mass of the object causing the lensing can be obtained. (The mass determination is model dependent, relying on the value of the Hubble constant, H_0, and the spacetime geometry.) There are three types, strong, weak and micro-lensing, the first two provide direct evidence for dark matter:

  - Strong lensing involves the observed distortion of background galaxies into arcs, producing multiple images of the galaxies. This occurs when the light passes through a very large object such as a large galaxy, and provides strong evidence for dark matter in galaxies.
  - Weak lensing involves the observation of minute distortions of images of galaxies due to foreground objects. By examining the apparent shear deformation of the adjacent background galaxies, one can characterize the mean distribution of dark matter statistically. This technique provides evidence for dark matter in galaxy clusters over and above that associated with the galaxies themselves.

- The motions of galaxies and gas in clusters (particularly the Bullet Cluster [7]);
- CMB (Cosmic Microwave Background) peak structure;
- (early) formation of structure in the universe.
- Galactic rotation curves: spiral galaxies do not exhibit the inverse square root rotation velocity fall off outside the observed galactic bulge expected from Keplerian dynamics. This indicates that they have a large invisible "halo" of matter outside this region.

It is these rotation curves, regarded as one of the key pieces of evidence for dark matter which are the focus of this project.

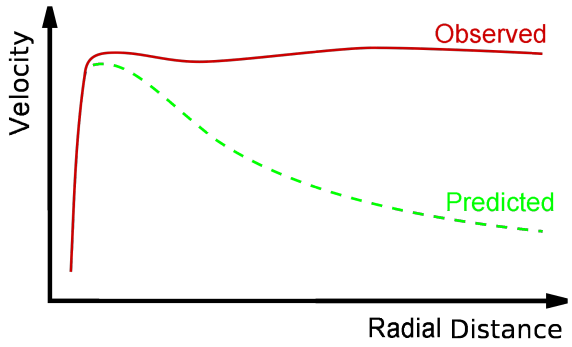

Figure 1.1: Rotation curve of a typical spiral galaxy. The discrepancy between the curves is attributed to dark matter. (*Image credit: Phil Hibbs*)

The ΛCDM concordance model assumes the Friedmann-Lemaître-Robertson-Walker (FLRW) spacetime metric, which describes a homogeneous, isotropic universe. It is best fit by a very close to spatially flat geometry with a curvature parameter $\Omega_k = 0.0125^{+0.0064}_{-0.0067}$ [8]. In the standard framework, the dynamics of bound systems are decoupled from cosmological expansion, and Kepler's Laws and the virial theorem of Newtonian mechanics are used to describe the motions of stars and galaxies.

Big bang nucleosynthesis combined with observations of the light element abundances (Fig 1.2)– in particular of deuterium, helium and lithium isotopes – strongly constrains the density of ordinary baryonic matter in the universe relative to the density of photons. In addition, the ratio of the heights of the Dopler peaks in the cosmic microwave background (CMB) anisotropy spectrum directly constrains the density of baryons relative to the total matter density. These combined observations indicate that the amount of baryonic matter is far smaller than the amount of nonbaryonic dark matter.

When one fits the cosmological parameters of ΛCDM one obtains that $\frac{\Omega_C}{\Omega_C+\Omega_B} = 83\%$ [8] of the matter in the universe is "exotic" nonbaryonic dark matter. There exists an alternative model, the timescape cosmology [9], which does not assume a homogeneous universe or feature a cosmological constant. Ratios of around 3:1 nonbaryonic to baryonic matter are

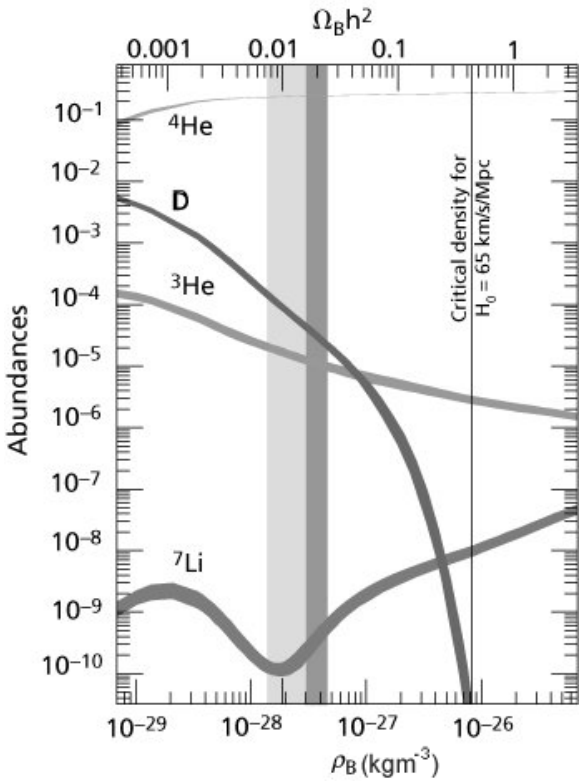

Figure 1.2: Predicted abundances of the main four light elements, as a function of the baryon density in the universe. The vertical bands indicate the observationally allowed regions, the darker band is a strong interpretation of the observational data, and the combined light and dark bands are a more conservative interpretation. (*Image credit: Michael S. Turner* [12])

typically found as a best fit in this model [10, 11], using boundary conditions consistent with the CMB anisotropies and primordial inflation.

In all current models such dark matter behaves like and is modelled by a perfect fluid, having no internal resistance or viscosity and isotropic pressure [13]. This requires that dark matter particles do not interact with each other except via gravity, and thus, for example, cannot emit or absorb photons or have electromagnetic charge.

1.2 Use of General Relativity

General relativity is the accepted theory of gravitation, having passed every experimental and observational test to date, with Newtonian gravity as its approximation where appropriate. This raises the question, why are we using Newtonian dynamics rather than general relativity to predict rotation velocities? Applying Occam's razor, could it be that Newtonian dynamics is not a valid approximation in this case and dark matter is not needed to explain the curves? As Newtonian dynamics is far simpler, it is more commonly used. For instance there is still no closed-form solution to the two-body problem in general relativity.

In the case of galactic rotation curves, it has been assumed that Newtonian dynamics is a valid approximation for a variety of reasons. The motions of stars are at nonrelativistic speeds, and apart from regions deep in the core of a galaxy which may contain black holes, the gravitational fields are weak as the average density of matter in a galaxy is low.

However, stars in galaxies are in motion under gravity alone. Such a system is known as "gravitationally bound" and it has been known since the time of Eddington that such a system yields nonlinear equations of motion in general relativity, as opposed to the linear equations of Newtonian theory. This is true in the time dependent case and Cooperstock and Tieu [14] also find it to be true in the stationary (non-time dependent) case.

It is well accepted by the community that there are many situations where general relativity is required, for instance, if a black hole is present. It is now believed that most, if not all, galaxies contain supermassive black holess at their centre [15] and observations from the last 15 years indicate that gas clouds and stars with relativistic velocity ($\sim 10^7 \mathrm{ms}^{-1}$) exist around the centre of various galaxies, including spiral galaxies [16]. Even for weak fields however, the many body system in general relativity has extra problems over and above that of Newtonian gravity. Gravitational energy is a concept which is not well-defined in Einstein's theory, and the meaning of which is still much debated. In Newtonian theory there is a fixed absolute space background and gravitational potentials are additive. That is to say, gravity is a conservative force. However, in general relativity matter creates its own background and one cannot simply superimpose two solutions without potentially changing the background geometry itself.

1.3 Existing models

Recently, attempts have been made to take to model galaxies with general relativity (GR). In 2006 Cooperstock and Tieu [14] (CT) used a cylindrically symmetric rotating dust solution to model spiral galaxies. Spiral galaxies are better able to fit to such a symmetry than say, irregular or elliptical galaxies, are abundant in the universe, and modelled with large halos of dark matter in the ΛCDM model. Cooperstock and Tieu consider within the context of GR a uniformly rotating fluid without pressure which is symmetric about its axis of rotation. This is a very simplified "toy" model, but it is solvable and one may hope to obtain some information about any differences in behaviour between GR and Newtonian dynamics from examining it. Another paper was published in 2008 by Balasin and Grumiller [17] (BG) which focused on the same method but attempted to address some of the many critiques of the CT model. In this project we attempt to isolate and fix some technical flaws of both of these models.

The general form for the stationary axially symmetric metric with the speed of light, $c = 1$ is [18]

$$ds^2 = e^{\nu-w}(udz^2 + dr^2) + r^2 e^{-w} d\phi^2 - e^w (dt - N d\phi)^2,$$

where u, ν, w and N are functions of cylindrical polar radial coordinate r, and axial coordinate z. We will show in Section 2.1 that one can set $u = 1$, $e^w = 1$ without lost of generality. Cooperstock and Tieu make an additional simplification, $e^\nu = 1$, which is not made by Balasin and Grumiller. Of the five Einstein equations, two key ones are:

$$\frac{{N_r}^2 + {N_z}^2}{r^2} = 8\pi G \rho e^\nu, \tag{1.1}$$

$$N_{rr} + N_{zz} - \frac{N_r}{r} = 0, \tag{1.2}$$

where ρ is the matter density of the galaxy, and the two models differ in whether they include e^ν. Cooperstock and Tieu also give the tangential velocity of matter in the galaxy as

$$V = r\omega = -\frac{g_{\phi t}}{g_{\phi\phi}} = \frac{rNce^w}{r^2 e^{-w} - N^2 e^w} \approx \frac{N}{r}, \tag{1.3}$$

when $r \gg N$. We find (c.f. 4.1.2) that $r\omega$ is not the invariant tangential velocity, which is N/r everywhere. Equations (1.1) and (1.3) give a relationship between density and velocity.

Both models use the ansatz that $N(r, z)$ is separable and write

$$N(r, z) = R(r)Z(z).$$

Equation (1.2) then implies

$$Z_{zz} = \pm k^2 Z.$$

Together with the reflection symmetry, $Z(z) = Z(-z)$, this implies that there are four possible forms of $Z(z)$: $e^{\pm k|z|}$, $\cos(kz)$, $\cosh(kz)$. With the further restriction that rotation velocity, and thus $N(r, z)$, not blow up as z becomes large this leaves two possibilities, $e^{-k|z|}$ and $\cos(kz)$. Cooperstock and Tieu use $Z(z) = e^{-k|z|}$, yielding, from (1.2)

$$R(r) = CJ_1(kr),$$

where C is a constant and J_1 is a Bessel function of the first kind. They then exploit the linearity of (1.2) and write the velocity as a linear superposition

$$N = -\sum_n k_n r C_n e^{-k_n|z|} J_1(k_n r), \tag{1.4}$$

where the k_n are chosen to be zeroes of $J_1(k_n r_0)$ for some r_0 which roughly corresponds to the galaxy radius, in order for these terms to form an orthogonal basis. They apply this formula in fitting to the rotation curves of four spiral galaxies, and find that a sum of ten terms is required to obtain a sufficiently good fit to the data.

Balasin and Grumiller, however, argue that $e^{-k|z|}$ is nonsmooth at $z = 0$ and this is unphysical behaviour (discussed further in 4.2.1), so one must instead use $Z(z) = \cos kz$, they are led to solutions involving modified Bessel functions rather than ordinary ones. Instead of a discrete sum of terms, they integrate over all possible modes, to obtain:

$$N(r, z) = \int_0^\infty dk\, C(k)\, k\, r\, K_1(kr) \cos(kz), \tag{1.5}$$

where $C(k)$ is an arbitrary function. They then impose a boundary condition at $r = 0$, which results in N being

$$N(r, z) = V_0(R - r_0) + \frac{V_0}{2} \sum_\pm \left[\sqrt{(z \pm r_0)^2 + r^2} - \sqrt{(z \pm R)^2 + r^2} \right], \tag{1.6}$$

for some constants V_0, r_0, R. (We find this boundary condition to be unsuitable in Section 4.1.3.)

It is possible that Cooperstock and Tieu's choice of z dependence could be used with the integral formulation, or Balasin and Grumiller's with a linear superposition of orthogonal terms. We investigate this in Section 4.2.1.

1.4 Contributions

In this project we analyse and extend the two models and check for and attempt to correct technical flaws. My main contributions are:

- Confirming the results of Ref. [14], extending their analysis to produce similar fits using a larger data set with more accurately measured rotation curves in Section 2.3;
- Calculating the asymptotic forms of the density in the limit of large r and z, and comparing this to empirical density profiles in Section 3.1;
- Checking whether one can recover the metric of flat space at spatial infinity in either of the models in Section 3.2;
- Verifying that the continuous integral can be used for Cooperstock and Tieu's choice of $Z(r)$ as in the work of Balasin and Grumiller in Section 4.2.1;
- Finding that an asymptotic density profile matched to the empirically found one can satisfy the Einstein field equations in Section 4.2.3;
- Attempting to replace the faulty boundary condition of Ref. [17] with the condition $\rho = 0$ on the surface $N = r$, which led to the discovery that the separation ansatz used in both models yields contradictions in Section 4.2.4.

Chapter 2

The Cooperstock–Tieu Model

2.1 Einstein's Equations

The Einstein field equations without cosmological constant can be written as

$$G_{\mu\nu} = R_{\mu\nu} - \frac{1}{2}Rg_{\mu\nu} = 8\pi G T_{\mu\nu},$$

where $G_{\mu\nu}$ is a symmetric second rank tensor in four dimensions, $T_{\mu\nu}$ is the stress-energy tensor and G is the gravitational constant, $G = 6.67384 \times 10^{-11}\mathrm{m}^3\mathrm{kg}^{-1}\mathrm{s}^{-2}$. This gives a system of ten coupled, nonlinear, hyperbolic-elliptic partial differential equations. The Einstein tensor, $G_{\mu\nu}$, is constructed from the metric, $g_{\mu\nu}$, and its first and second derivatives, which enter into the Riemann curvature tensor, $R^{\mu}{}_{\nu\lambda\rho}$, and its contractions the Ricci tensor $R_{\mu\nu} = R^{\lambda}{}_{\nu\lambda\rho}$ and the Ricci scalar, $R = R^{\lambda}{}_{\lambda}$.

For the metric

$$ds^2 = e^{\nu-w}(udz^2 + dr^2) + r^2e^{-w}d\phi^2 - e^{w}(dt - Nd\phi)^2, \tag{2.1}$$

we use Maple to find the components of the Einstein tensor, $G_{\mu\nu}$:

- $G_{tt} = 8\pi G T_{tt} = 8\pi G {g_{tt}}^2 T^{tt}$ yields

$$8\pi G\rho e^{\nu} = w_{rr} + w_{zz} + \frac{w_r}{r} - \frac{1}{4}({w_r}^2 + {w_z}^2) + \frac{3e^{2w}}{4r^2}({N_r}^2 + {N_z}^2) - \frac{1}{2}(\nu_{rr} + \nu_{zz}). \tag{2.2}$$

- $G_{t\phi} = 8\pi G T_{t\phi} = 8\pi G g_{tt} g_{t\phi} T^{tt}$ yields

$$\begin{aligned} 8\pi G\rho e^{\nu} = {} & w_{rr} + w_{zz} + \frac{w_r}{r} - \frac{1}{4}({w_r}^2 + {w_z}^2) + \frac{3e^{2w}}{4r^2}({N_r}^2 + {N_z}^2) - \frac{1}{2}(\nu_{rr} + \nu_{zz}) \\ & + \frac{1}{N}\left[\frac{1}{2}(N_{rr} + N_{zz} - \frac{N_r}{r}) + N_r w_r + N_z w_z\right]. \end{aligned} \tag{2.3}$$

- $G_{\phi\phi} = 8\pi G T_{\phi\phi} = 8\pi G g_{t\phi}^2 T^{tt}$ yields

$$\begin{aligned} 8\pi G\rho e^{\nu} = {} & w_{rr} + w_{zz} + \frac{w_r}{r} - \frac{1}{4}({w_r}^2 + {w_z}^2) + \frac{3e^{2w}}{4r^2}({N_r}^2 + {N_z}^2) - \frac{1}{2}(\nu_{rr} + \nu_{zz}) \\ & + \frac{1}{N}[(N_{rr} + N_{zz} - \frac{N_r}{r}) + 2(N_r w_r + N_z w_z)] \\ & + \frac{1}{4N^2}[{N_r}^2 + {N_z}^2 + r^2e^{-2w}({w_r}^2 + {w_z}^2 + 2(\nu_{rr} + \nu_{zz}))]. \end{aligned} \tag{2.4}$$

- $G_{rz} = 0$ yields

$$r^2 w_r w_z - r\nu_r - e^{2w} N_r N_z = 0. \tag{2.5}$$

- $G_{rr} = 0, G_{zz} = 0$ yields

$$e^{2w}({N_r}^2 - {N_z}^2) + 2r\nu_r - r^2({w_r}^2 - {w_z}^2) = 0. \tag{2.6}$$

These give

$$(2.3) - (2.2) = N_{rr} + N_{zz} - \frac{N_r}{r} + 2(N_r w_r + N_z w_z) = 0 \tag{2.7}$$

$$(2.7) \implies (2.4) - (2.3) = 2(\nu_{rr} + \nu_{zz}) + {w_r}^2 + {w_z}^2 + \frac{e^{2w}}{r^2}({N_r}^2 + {N_z}^2) = 0. \tag{2.8}$$

These equations will not all be independent on account of the Bianchi identities.

Cooperstock and Tieu work in the frame that is comoving with the matter, which yields $w_r = 0$ and $w_z = 0$ from the geodesic equations. They then, like van Stockum [18], without loss of generality take $w = 0$, which was found to be equivalent to normalisation the 4-velocity $U^\mu U_\mu = g_{00} = -e^w = -1$. They also set $u = 1$, with the rationale that higher order terms in a series expansion of u would lead to terms of order G^n, where $n \geq 1$, in the field equations, which are negligible. The perturbative equations of [14] follow by also taking $e^\nu = 1$ and only keeping derivatives of w which are linear; this includes taking terms $N_r w_r$ to be nonlinear and also discarding these.

So Einstein's equations are reduced to:

$$(2.6) \implies 2r\nu_r + {N_r}^2 - {N_z}^2 = 0, \tag{2.9}$$

$$(2.5) \implies r\nu_z + N_r N_z = 0, \tag{2.10}$$

$$(2.8) \implies {N_r}^2 + {N_z}^2 + 2r^2(\nu_{rr} + \nu_{zz}) = 0, \tag{2.11}$$

$$(2.7) \implies N_{rr} + N_{zz} - \frac{N_r}{r} = 0, \tag{2.12}$$

$$(2.2) \implies \frac{{N_r}^2 + {N_z}^2}{r^2} = 8\pi G\rho e^\nu. \tag{2.13}$$

This matches the equations in both papers (with $e^\nu = 1$ in [14]).

2.2 Bessel calculation

From equation (2.12), if the separation ansatz $N(r, z) = R(r)Z(z)$ is used, and we have a z dependence of $e^{-k|z|}$, then $N_{zz} = k^2 N$, giving the ordinary differential equation

$$R'' + k^2 R - \frac{R'}{r} = 0. \tag{2.14}$$

We can then check that the solution given in [14], $R(r) = rJ_1(kr)$, indeed satisfies (2.14), where J_1 is a Bessel function of the first kind. We use the identities

$$\frac{d}{dx}y_p(\alpha x) = \alpha y_{p-1}(\alpha x) - \frac{p}{x}y_p(\alpha x),$$
$$\frac{d}{dx}y_p(\alpha x) = -\alpha y_{p+1}(\alpha x) + \frac{p}{x}y_p(\alpha x),$$

which apply to any Bessel function of the first or second kind, Hankel functions and modified Bessel functions of the first kind, to obtain

$$\frac{d}{dr}J_1(kr) = kJ_0(kr) - \frac{1}{r}J_1(kr),$$
$$\frac{d}{dr}J_0(kr) = -kJ_1(kr).$$

It follows that

$$R(r) = rJ_1(kr), \tag{2.15}$$
$$R'(r) = krJ_0(kr), \tag{2.16}$$
$$R''(r) = kJ_0(kr) - k^2rJ_1(kr). \tag{2.17}$$

Substituting (2.15), (2.16) and (2.17) into (2.14):

$$kJ_0(kr) - k^2rJ_1(kr) + k^2rJ_1(kr) - kJ_0(kr) = 0,$$

as required. In fact, any linear combination of $rJ_1(kr)$ and $rY_1(kr)$, where Y_1 is a Bessel function of the second kind, would satisfy (2.14) but as we want N to be finite at $r = 0$, the coefficient of the $rY_1(kr)$ term must be set equal to zero.

2.3 Rotation curves

The values of the coefficients k_n (which all depend on an single r_0 which can be calculated) and C_n which give the best fit to the observed velocities were provided in the appendix of Ref. [14]. Using the same velocity data from the four galaxies, the Milky Way, NGC3031, NGC 3198 and NGC7331, which Cooperstock and Tieu used in producing their rotation curves for these galaxies, we were able to produce fits to this data which gave coefficients matching, or very close to, those of [14]. In the cases where the coefficients were not an exact match, a least squares comparison revealed that our fits were slightly better. For some of these, we found that several data points had to be removed to achieve this (the first point for the Milky Way, the first 3 points for NGC 3198, and the first and last points for NGC 7331, ones not shown on their plots), and that adding these extra terms gave a worse fit. It was confirmed [19] that Cooperstock and Tieu had not used these datapoints, with the justification that to obtain a flat velocity curve, the plot should be mostly composed of "low-frequencies" (i.e., small k_n values) and keeping the first few points requires the velocity to jump from 0 to the order of 200 km/sec within 1kpc. To model this requires "high frequency" terms and the point of the model is to keep a small number of k_n's. It was also added that the importance of the points in integrating the mass scales as r^2 making the first points less important. However, perhaps Cooperstock and Tieu should have used a weighted fit rather than removing datapoints for this purpose. They did not address why the last point of NGC7331 was removed.

We found that Ref. [14] had used integer values for r_0, and we were able to obtain better fits by adding r_0 as a parameter and optimising its value. It was also discovered that one of the galaxies Cooperstock and Tieu had fitted, NGC3031, was "dominated by non-circular motions" [20], making it an unfit candidate for a modelling with circular symmetry.

Using the same Python program (c.f. Appendix B) we extended this analysis by producing fits using better data from the THINGS dataset [21]. This data is more recent, includes error bars (the original data did not) and contained fifteen spiral galaxies. The program was adjusted to take into account the uncertainties and we also used a χ^2 minimising fit rather than the least squares fit used in [14]. We found a reduced χ^2 usually much less than one for most galaxies, indicating an extremely good fit. However, this was not the case for very large galaxies. The number of terms in the sum was varied up to twenty for these large galaxies. At twenty terms we could get a reduced χ^2 of around one for NGC5055. However, bumps far from the centre of the galaxy in these large galaxies are often due to shock fronts in the arms of the galaxy [22], therefore one would not want to fit very closely to these areas, as they do not obey the assumption of cylindrical symmetry in the model well.

We then proceeded to compare the reduced χ^2 of our CT model fit to ΛCDM Nevarro, Frenk and White halo (NFW) and isothermal halo fits with values of $\Upsilon_\star^{3.6}$ (stellar mass-to-light ratio in the 3.6 μm band) derived from the Kroupa initial mass function (IMF), the

Salpeter IMF, or with $\Upsilon_\star^{3.6}$ as a free parameter. We also compared them to our fit to the MOND parameters using equations (3) and (4) from [23], taking the MOND acceleration constant, a_0, as a free parameter or with $a_0 = 1.0 \times 10^{-8}$cm s^{-2} as in Swaters, Sanders and McGaugh [23] (SSM) or $a_0 = 1.22 \times 10^{-8}$cm s^{-2} as in Gentile, Fameay and de Blok [20] (GFdB).

Model	10 parameters	5 parameters
Isothermal, fixed Salpeter	14	8
Isothermal fixed Kroupa	13	9
Isothermal, free	12	6
NFW, fixed Salpeter	13	8
NFW, fixed Kroupa	12	7
NFW, free	12	6
MOND, a_0 fixed SSM	14	10
MOND, a_0 fixed GFdB	11	8
MOND, a_0 free	12	7

Table 2.1: Number of galaxies (of 15) for which the CT reduced χ^2 is lower

Table 2.1 shows that the ten parameters used by Cooperstock and Tieu gives better fits in almost all cases, and the number of parameters used needs to be reduced to five to achieve approximately equivalent goodness of fit to the ΛCDM models. (For details of the comparison see Appendix A.) However, such a comparison was discovered to be unfair, as the NFW and isothermal halo fits were obtained by fitting to observed densities and comparing the calculated rotations curves to observation, rather than fitting directly to the rotation curves. Cooperstock and Tieu do not appear to have highlighted that their plots of the rotation curve fits alone do not say much about the predictive success of the model.

We used (1.4) and (2.13) to obtain an expression for the density:

$$\rho = 8.36 \times 10^5 \left[\left(\sum_{n=1}^{10} k_n^2 C_n e^{-k_n|z|} J_0(k_n r) \right)^2 + \left(\sum_{n=1}^{10} k_n^2 C_n e^{-k_n|z|} J_1(k_n r) \right)^2 \right] \frac{M_\odot}{pc^3}.$$

In order to judge to predictive success of the CT model one would have use this relation with the coefficients produced in the velocity fit and compare the calculated density profile with the observed densities. Conversely, one could fit to observed densities to obtain the coefficients and from this calculate the velocities and compare these to observed rotation curves. Neither comparison was made in [14].

We discovered the former comparison had already been made by Fuchs and Phleps [24], for the Milky Way. They found that the CT model predicted densities lower than observed in the interior and higher than observed on the surface. The total mass predicted by the CT model was consistent with observation. While the prediction of a higher density than observed one can always be attributed to dark matter, prediction of *lower* densities in any region contradicts observation and this problem would render the CT model in its original form unworkable. However, this was only for one galaxy and as an extension of this work – which we have not investigated – we could calculate the density for all the THINGS dataset spiral galaxies (minus NGC3031) to check if it is the case for any of them, and if so, calculate how much lower a density it predicts than is observed.

On the following pages are fits to the rotation velocity of fourteen of the galaxies using data from the THINGS dataset.

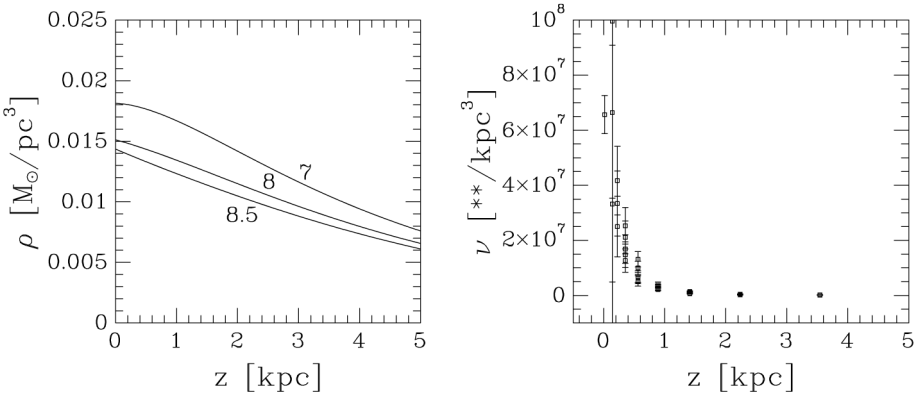

Figure 2.1: Predicted versus observed vertical distribution of the mass density in the Milky Way at the position of the Sun. (Left panel) Vertical distribution predicted by the mass model of Cooperstock and Tieu. The profiles are labelled by the assumed galactocentric distance of the Sun ranging from 7 to 8.5 kpc. (Right panel) The observed distribution of stars perpendicular to the galactic midplane. (*Image Credit: B. Fuchs, S. Phleps.* [24])

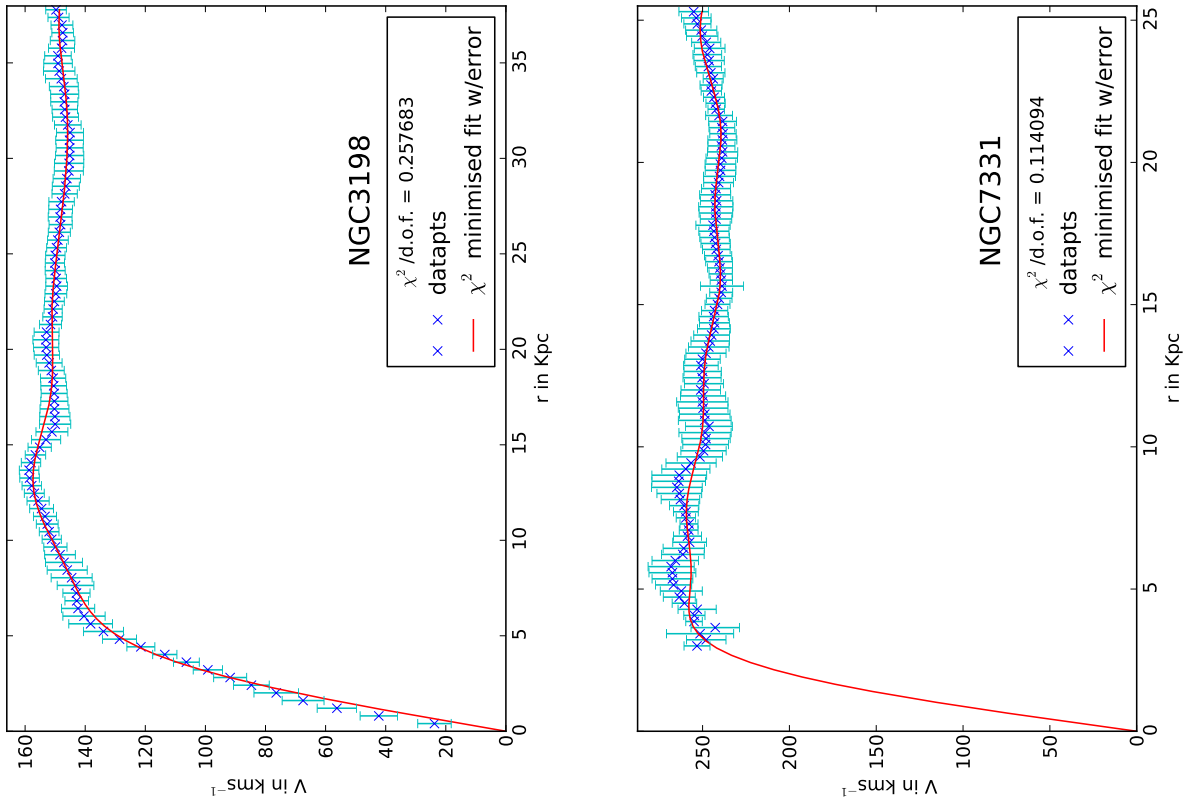

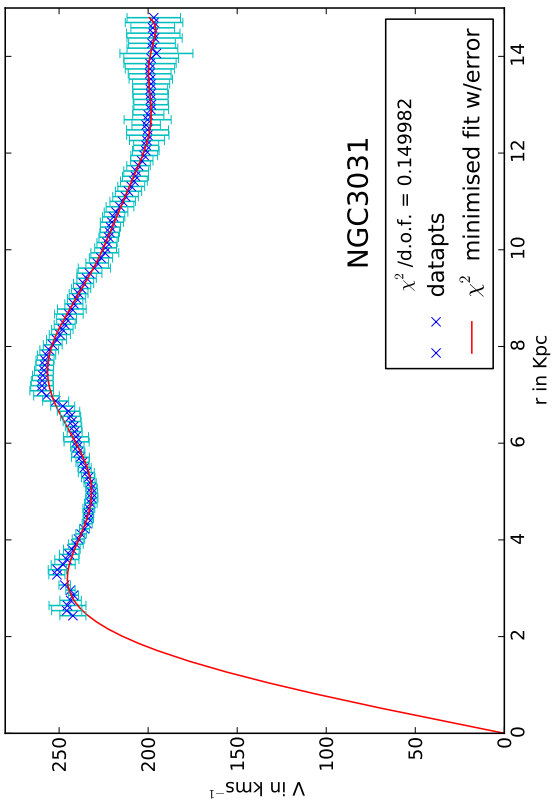
NGC3031
χ^2/d.o.f. = 0.149982
datapts
χ^2 minimised fit w/error
V in kms^{-1}
r in Kpc

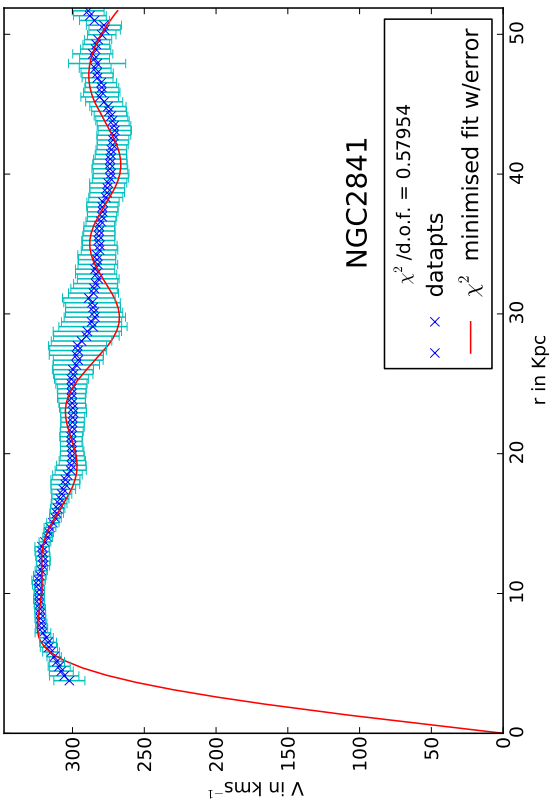
NGC2841
χ^2/d.o.f. = 0.57954
datapts
χ^2 minimised fit w/error
V in kms^{-1}
r in Kpc

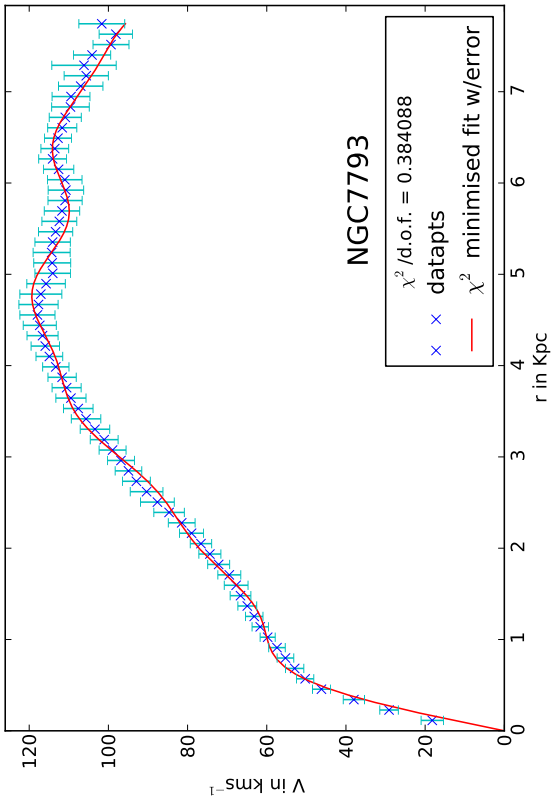
NGC7793
χ^2/d.o.f. = 0.384088
datapts
χ^2 minimised fit w/error
V in kms^{-1}
r in Kpc

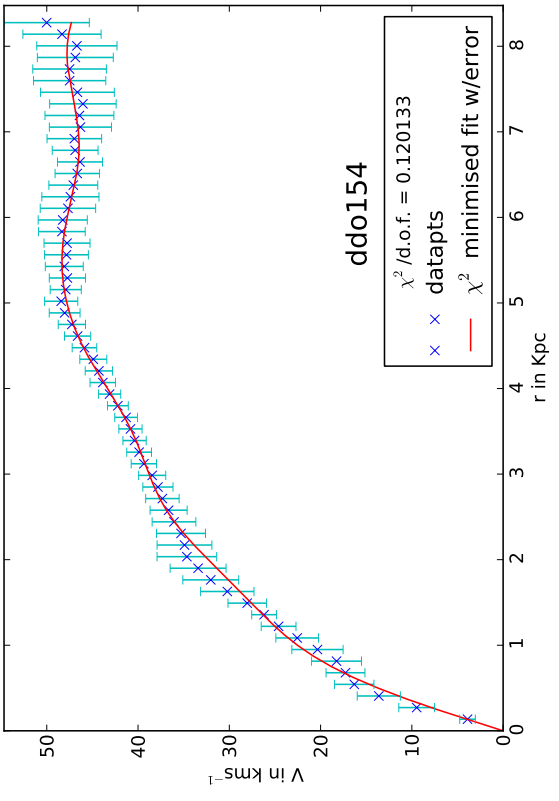
ddo154
χ^2/d.o.f. = 0.120133
datapts
χ^2 minimised fit w/error
V in kms^{-1}
r in Kpc

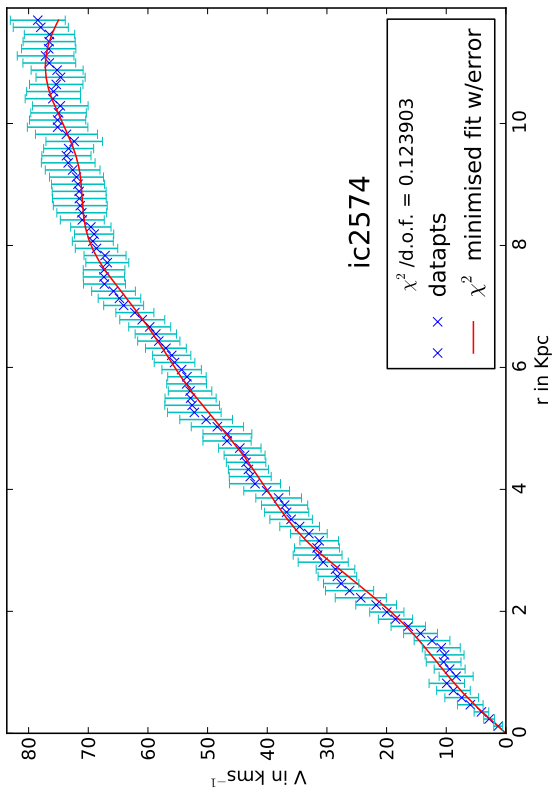
ic2574
χ^2 /d.o.f. = 0.123903
datapts
χ^2 minimised fit w/error
V in kms^{-1}
r in Kpc

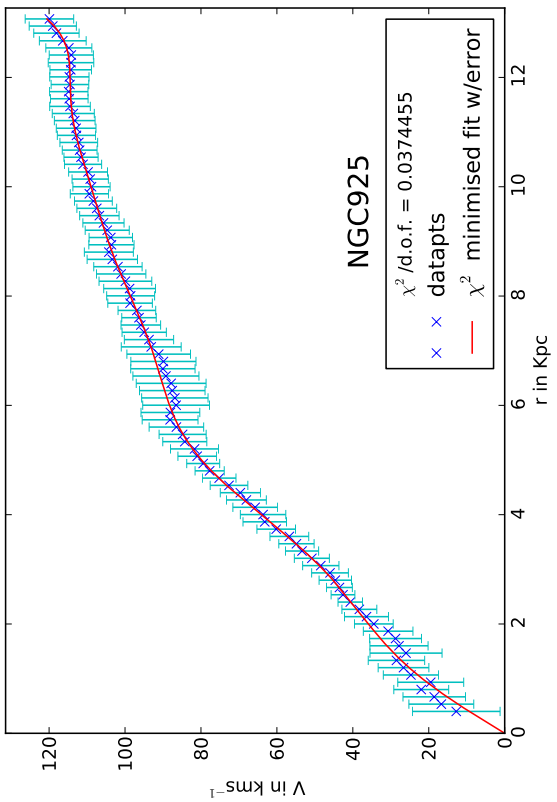
NGC925
χ^2 /d.o.f. = 0.0374455
datapts
χ^2 minimised fit w/error
V in kms^{-1}
r in Kpc

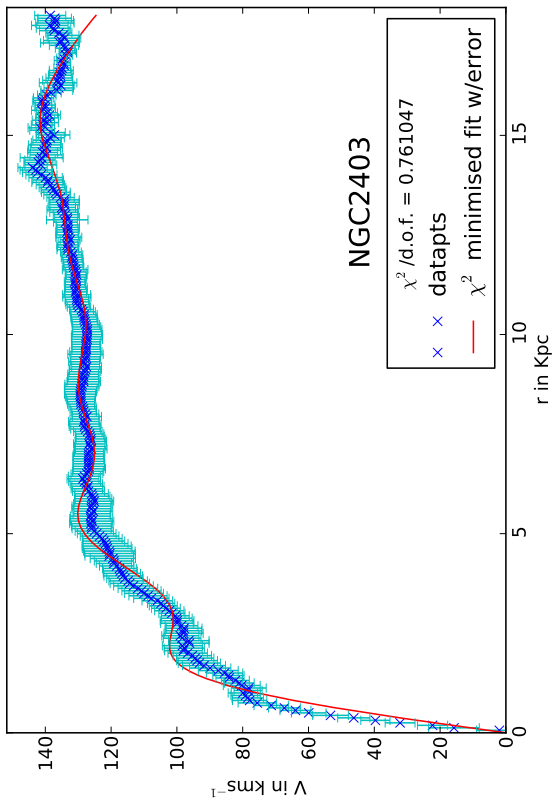
NGC2403
χ^2 /d.o.f. = 0.761047
datapts
χ^2 minimised fit w/error
V in kms^{-1}
r in Kpc

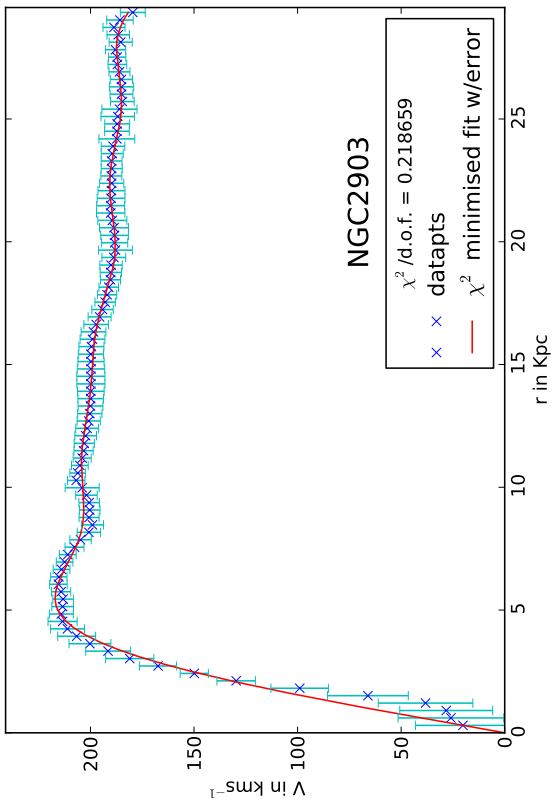
NGC2903
χ^2 /d.o.f. = 0.218659
datapts
χ^2 minimised fit w/error
V in kms^{-1}
r in Kpc

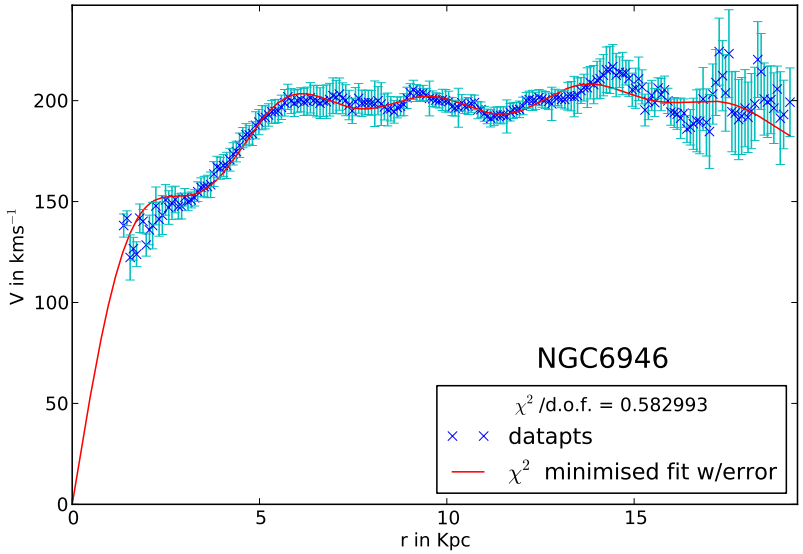
NGC6946
χ^2 /d.o.f. = 0.582993
datapts
χ^2 minimised fit w/error
V in kms^{-1}
r in Kpc

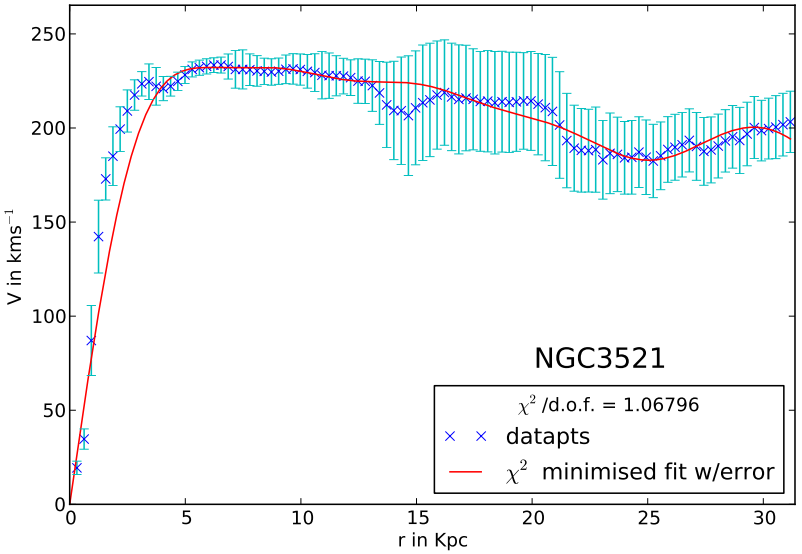
NGC3521
χ^2 /d.o.f. = 1.06796
datapts
χ^2 minimised fit w/error
V in kms^{-1}
r in Kpc

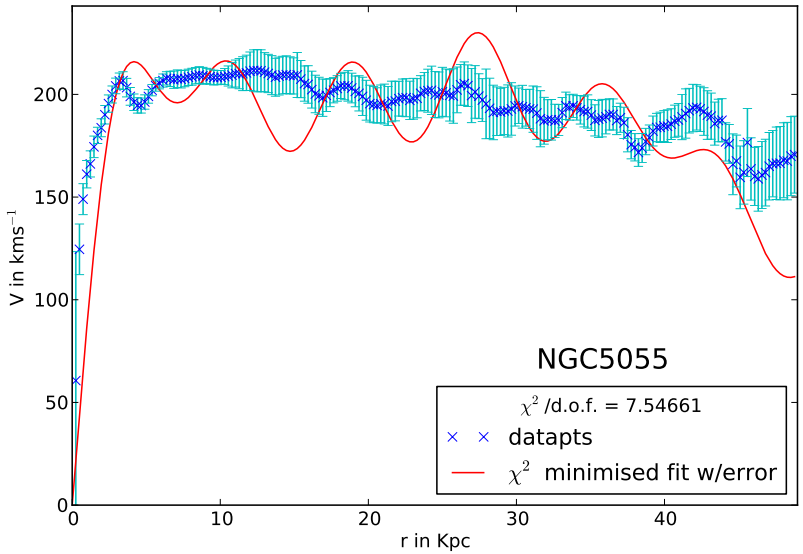
NGC5055
χ^2 /d.o.f. = 7.54661
datapts
χ^2 minimised fit w/error
V in kms^{-1}
r in Kpc

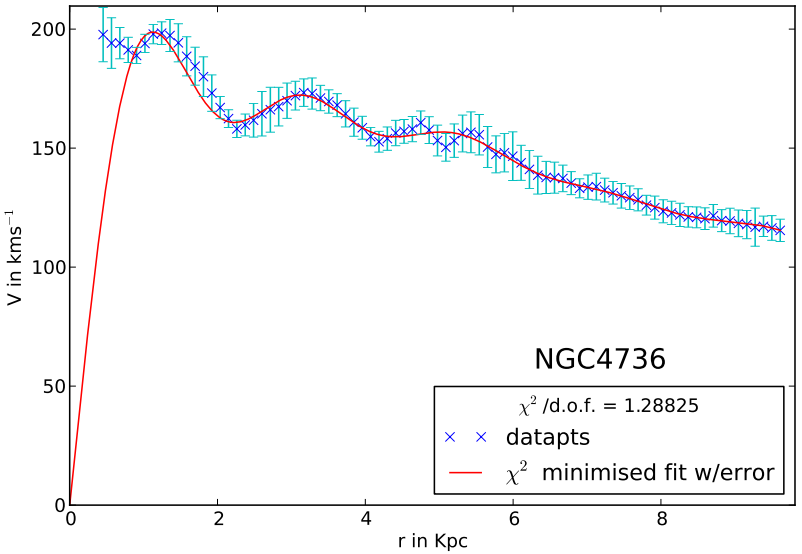
NGC4736
χ^2 /d.o.f. = 1.28825
datapts
χ^2 minimised fit w/error
V in kms^{-1}
r in Kpc

Chapter 3

Asymptotic Behaviour of the Models

We are interested in the behaviour of the models at spatial infinity for reasons of mathematical consistency. The following analysis was not done by Cooperstock and Tieu. Some analysis of the asymptotic behaviour of the density was done by Balasin and Grumiller.

3.1 Metric Behaviour

3.1.1 BG Model

The following analysis is using the final form of $N(r,z)$ Balasin and Grumiller derived by imposing

$$A(\lambda) = \frac{2}{\pi}\int_0^\infty dx C(x)\cos(\lambda x), \tag{3.1}$$

with

$$C(x) = (x-r_0)\theta(x-r_0) - \theta(x-R)) + (R-r_0)\theta(x-R), \tag{3.2}$$

where θ is the step function, V_0 is a constant and r_0, R are parameters.

We require that the metric of any solution match that of Minkowski flat space at spatial infinity in either the r or z direction. The metric given in [17] is

$$ds^2 = e^\nu(dz^2+dr^2) + r^2 d\phi^2 - (dt - N d\phi)^2, \tag{3.3}$$

which we wish to match to

$$ds^2 = dz^2 + dr^2 + r^2 d\phi^2 - dt^2, \tag{3.4}$$

either in the original coordinates r and z, or under a suitable coordinate transformation.

First we examine the BG model. The form of N derived in [17] is

$$N(r,z) = V_0(R-r_0) + \frac{V_0}{2}\sum_{\pm}\left[\sqrt{(z\pm r_0)^2+r^2} - \sqrt{(z\pm R)^2+r^2}\right]. \tag{3.5}$$

At large z we have, using the binomial theorem,

$$N(r,z) = V_0(R-r_0) + \frac{V_0}{2}\sum_{\pm} z\left[\sqrt{1 \pm \tfrac{2r_0}{z} + \tfrac{r_0^2}{z^2} + \tfrac{r^2}{z^2}} - \sqrt{1 \pm \tfrac{2R}{z} + \tfrac{R^2}{z^2} + \tfrac{r^2}{z^2}}\right] \tag{3.6}$$

$$\approx V_0(R-r_0) + \frac{V_0}{2}\sum_{\pm} z\Bigg[\left(1 \pm \tfrac{2r_0}{z} + \tfrac{1}{2z^2}\left(r_0^2+r^2\right) - \tfrac{1}{4z^2}\left(\pm 2r_0 + \tfrac{r_0^2}{z} + \tfrac{r^2}{z}\right)^2\right) - \left(1 \pm \tfrac{2R}{z} + \tfrac{1}{2z^2}\left(R^2+r^2\right) - \tfrac{1}{4z^2}\left(\pm 2R + \tfrac{R^2}{z} + \tfrac{r^2}{z}\right)^2\right)\Bigg]$$

$$= V_0(R-r_0) + \frac{V_0}{2z}(R^2-r_0^2)\left(1 + \frac{r^2+1/2}{z^2}\right) \tag{3.7}$$

$$\to V_0(R-r_0) \quad \text{as } z \to \infty. \tag{3.8}$$

And at large r, again using binomial theorem, we have

$$N(r,z) \approx V_0(R-r_0) + \frac{V_0}{2}\sum_{\pm} r\left[1 + \frac{1}{2}\left(\frac{z \pm r_0}{r}\right)^2 - \frac{1}{8}\left(\frac{z \pm r_0}{r}\right)^4 - 1 - \frac{1}{2}\left(\frac{z \pm R}{r}\right)^2 + \frac{1}{8}\left(\frac{z \pm R}{r}\right)^4\right] \tag{3.9}$$

$$= V_0(R-r_0) + \frac{V_0}{2r}\left[(r_0^2-R^2) + \frac{1}{4r^3}\left(r_0^2(r_0^2+6z^2) - R^2(R^2+6z^2)\right)\right] \tag{3.10}$$

$$\to V_0(R-r_0) \text{ as } r \to \infty. \tag{3.11}$$

Therefore $N(r,z)$ approaches the constant value $V_0(R-r_0)$ at spatial infinity. We can thus make the coordinate transformation to rotating coordinates:

$$dt \to dt' = dt + N d\phi. \tag{3.12}$$

We then require that $e^\nu \to 1$ i.e. $\nu \to 0$ as $r \to \infty$ and $z \to \infty$. First, we look at the behaviour of ν at large z. From (3.7), taking only the leading order term, we have

$$N(r,z) \approx V_0(R-r_0) + \frac{V_0}{2z}(R^2-r_0^2), \tag{3.13}$$

implying

$$N_r \sim \frac{r}{z^2} \text{ and } N_z \sim \frac{r^2}{z^3}.$$

Thus, from (2.10) in Einstein's equations,

$$\nu_z = \frac{N_r N_z}{r} \sim \frac{r^2}{z^4},$$

so that

$$\nu \sim \frac{r^2}{z^4} \to 0 \text{ as } z \to \infty.$$

Now we look at the behaviour of ν at large r. Using (3.10) and keeping only leading order terms in r and second order terms that involve z,

$$N(r,z) \approx V_0(R-r_0) + \frac{V_0(r_0^2-R^2)}{2r}\left[1 + \frac{3z^2}{2r^3}\right]. \tag{3.14}$$

Hence

$$N_r \sim \frac{1}{r^2} \text{ and } N_z \sim \frac{z}{r^4}.$$

From (2.9) in Einstein's equations

$$\nu_r \propto \frac{N_z^2 - N_r^2}{r} \sim \frac{1}{r}\left(\frac{1}{r^4} - \frac{1}{r^2}\right) \sim \frac{1}{r^5}, \tag{3.15}$$

so that

$$\nu \sim \frac{1}{r^4} \to 0 \text{ as } r \to \infty.$$

Hence the metric in the Balasin and Grumiller model with their boundary condition on N approaches the metric of flat space far from the centre of the galaxy.

3.1.2 CT Model

Next we examine the Cooperstock and Tieu model. Recall from (1.4) the expression for N in the CT model is

$$N = -Ckre^{-k|z|}J_1(kr).$$

Clearly N approaches a constant value of 0 as z become large. However, when $r \gg 1$,

$$J_0(kr) \approx \sqrt{\frac{2}{\pi kr}}\cos\left(kr - \frac{\pi}{4}\right), \tag{3.16}$$

$$J_1(kr) \approx \sqrt{\frac{2}{\pi kr}}\cos\left(kr - \frac{\pi}{4} - \frac{\pi}{2}\right) = \sqrt{\frac{2}{\pi kr}}\sin\left(kr - \frac{\pi}{4}\right). \tag{3.17}$$

And so $N \sim \sqrt{r}\sin\left(kr - \frac{\pi}{4}\right)$ which does not approach a constant value as $r \to \infty$.

Next we examine the behaviour of ν.

$$N_r = -Ck^2 rJ_0(kr)e^{-k|z|}, \tag{3.18}$$

$$N_z = Ck^2 rJ_1(kr)e^{-k|z|}. \tag{3.19}$$

From (2.10) in Einstein's equations, for large z,

$$\nu_z = \frac{N_r N_z}{r} \sim re^{-2k|z|} \tag{3.20}$$

$$\implies \nu \sim e^{-2k|z|} \to 0 \text{ as } z \to \infty. \tag{3.21}$$

From (2.9) in Einstein's equations and (3.16) and (3.17), for large r,

$$\nu_r \propto \frac{N_z^2 - N_r^2}{r} \sim \sin^2\left(kr - \frac{\pi}{4}\right) - \cos^2\left(kr - \frac{\pi}{4}\right) \tag{3.22}$$

$$\implies \nu \sim \cos(2kr) \nrightarrow 0 \text{ as } r \to \infty. \tag{3.23}$$

Thus we find that for Cooperstock and Tieu's solution the metric approaches the flat space metric far from the galaxy in the azimuthal direction but not in the radial direction.

3.2 Density Behaviour

3.2.1 CT Model density decay

We would expect a feasible expression for the density of a spiral galaxy to asymptotically approach the empirical density profile $\rho_N \propto \exp(-r/H)\exp(-z/h)$ [25], for some scale heights h and H, or something suitably close to it, in the limits $r \to \infty$ and $z \to \infty$. The

density derived in [14], ρ_{CT}, clearly decays as $\exp(-z/h)$ as $z \to \infty$. Here we check how fast it decays in the $r \to \infty$ limit. We have, from (2.13), (2.15) and (2.16),

$$\rho_{CT} \propto \frac{{N_r}^2 + {N_z}^2}{r^2} \propto \frac{1}{r^2}\left[\left(\frac{\partial}{\partial r}\left(rJ_1(kr)\right)\right)^2 + k^2\left(rJ_1(kr)\right)^2\right] \tag{3.24}$$

$$= k^2\left(J_0(kr)^2 + J_1(kr)^2\right). \tag{3.25}$$

Using (3.16) and (3.17), the density (3.25) becomes

$$\rho_{CT} \propto k^2\left[\left(\sqrt{\frac{2}{\pi kr}}\sin\left(kr - \frac{\pi}{4}\right)\right)^2 + \left(\sqrt{\frac{2}{\pi kr}}\cos\left(kr - \frac{\pi}{4}\right)\right)^2\right] = \frac{2k}{\pi r} \tag{3.26}$$

as $r \to \infty$. As a linear superposition of terms proportional to $1/r$ is still proportional to $1/r$, this does not decay as fast as $\exp(-r/H)$ in the asymptotic limit.

3.2.2 BG Model density decay

From (2.13) the density, after some simplification, and since $e^{-\nu} \to 1$ at infinity, is found to be

$$\rho \propto \frac{{N_r}^2 + {N_z}^2}{r^2} = \frac{2}{r^2}\sum_{\pm}\left[1 - \frac{r^2 + (z \pm r_0)(z \pm R)}{\sqrt{((z \pm r_0)^2 + r^2)((z \pm R)^2 + r^2)}}\right]. \tag{3.27}$$

As r or z tends to infinity the fraction in the brackets on the right becomes 1 so the density approaches zero.

To determine the behaviour of the density at spatial infinity we made the coordinate transformations $x = 1/z$ and $y = 1/r$ and then used Maple to find the Taylor series expansion about $x = 0$ of $\rho(r, x)$ and about $y = 0$ of $\rho(y, z)$ before transforming back to the original coordinates. The first two terms in the series about $x = 0$ are:

$$\rho(r, z) \approx \frac{V_0 e^{-\nu}}{\kappa}\left[\frac{2(r_0 - R)^2}{r^4} - \frac{(r_0 - R)^2}{2r^6}(3r_0^2 + 2r_0R + 3R^2 + 8z^2)\right] \tag{3.28}$$

$$\propto \frac{1}{r^4} \text{ as } r \to \infty. \tag{3.29}$$

Similarly about $y = 0$:

$$\rho(r, z) \approx \frac{V_0 e^{-\nu}}{\kappa}\left[\frac{2(r_0 - R)^2}{z^4} + \frac{(r_0 - R)^2}{2z^6}(3r_0^2 + 4r_0R + 3R^2 - 2r^2)\right] \tag{3.30}$$

$$\propto \frac{1}{z^4} \text{ as } z \to \infty. \tag{3.31}$$

Hence we do not obtain an exponential falloff of the density at large r and z. However, this falloff may be appropriately fast to give an empirically workable model, unlike a $1/r$ falloff. Incidentally, this calculation contradicts Balasin and Grumiller's statement that the density falls off like $1/r^6$ for $r \gg R$ [17].

Chapter 4

Boundary Conditions and Spacetime Geometry

4.1 Critiques

4.1.1 Proper Distances

We note that in both models the authors have treated the *coordinates* r and z as if they were the radial and axial *proper distances*, respectively. If the density is close to asymptotically flat then $dR \approx dr$, but if one is setting boundary conditions then one should take great care.

For example, if a typical profile is $\rho(R, Z) = \rho_0 e^{-R/H} e^{-Z/h}$, where R is the proper radius and Z is the proper height, the metric is:

$$\begin{aligned} ds^2 &= e^\nu (dz^2 + dr^2) + r^2 d\phi^2 - (dt - N d\phi)^2 \\ &= dR^2 + dZ^2 + r^2 d\phi^2 - (dt - N d\phi)^2, \end{aligned}$$

where $dR = e^{\nu/2} dr$, $dZ = e^{\nu/2} dz$ and r is implicitly defined. This means that $R = r$ and $Z = z$ far from the galaxy centre if $e^\nu \to 1$, but we need a solution for ν to find the proper distances in terms of r and z coordinates near the galaxy centre. The intrinsic problem of using r, z as coordinates is that the dust profile is given in proper distance units.

As we show later in Section 4.2.4,

$$\nu = -\frac{1}{2} \frac{R \frac{dR}{dr}}{r} Z^2. \tag{4.1}$$

Hence in the case of the CT model we have $e^{\nu/2} = \exp(-\frac{C^2 k^3}{4} r J_1(kr) J_0(kr) e^{-2k|z|})$ which decays to $e^{\nu/2} = 1$ for $z \neq 0$, but for $z = 0$ oscillates between two values for all r. However, for values of $k \sim 1$ and $Ck \sim 10^{-3}$ as typically found in [14], the amplitude of oscillation is very small, and we find numerically that the assumption that $e^\nu = 1$ is accurate to six decimal places, and the coordinate and proper distances are in fact very close.

In the case of the BG model we have $e^{\nu/2} = \exp(\frac{k^3}{4} r K_1(kr) K_0(kr) \cos^2(kz))$. As shown in Section 3.1.1 $e^\nu \to 1$ at large r and z, but $e^{\nu/2} \to \infty$ as $r \to 0$ (though we cannot look at the region $r < N$, c.f. Section 4.1.3). Therefore, the difference between proper and coordinate distance could be consequential when applying boundary conditions to the BG solution near the centre of the galaxy.

4.1.2 Invariant Velocity

A footnote in Ref. [14] states that "A referee has kindly indicated to us that the local tangential velocity can also be derived in an invariant manner." This is indeed the case, in general ωr would *not* be the local velocity of rotation. Here we derive the correct expression.

Bardeen [26] considers an observer moving on a circular trajectory, not necessarily co-moving with the dust, and writes the metric as

$$ds^2 = -e^{2\eta} dt^2 + e^{2\psi} (d\phi - \omega dt)^2 + e^{2\mu_r} dr^2 + e^{2\mu_z} dz^2, \tag{4.2}$$

where ψ and η are functions of r and z. The local expression for the velocity of such an observer is then found to be (Equation (38) of [26])

$$v = (\Omega - \omega)e^{\psi-\eta}, \tag{4.3}$$

The coordinate angular velocity, $\Omega = \frac{d\phi}{dt}$, is the angular velocity as measured by a distant stationary observer and ω is the angular velocity as seen from infinity of a locally nonrotating observer.

We can evaluate e^{ψ} and e^{η} for the particular case of the CT metric in order to obtain an expression for the velocity. With $e^{w} = 1$, we have

$$\begin{aligned} e^{2\psi}d\phi^2 &= (r^2 - N^2)d\phi^2 \\ \implies \quad e^{\psi} &= \sqrt{r^2 - N^2}. \end{aligned} \tag{4.4}$$

Also from equating the two metrics,

$$\begin{aligned} dt &= (e^{2\eta} - \omega^2 e^{2\psi})dt \\ \implies e^{2\eta} &= 1 + \omega^2 e^{2\psi} \\ &= 1 + \left(\frac{-N}{r^2 - N^2}\right)^2 (r^2 - N^2) \\ e^{2\eta} &= \frac{r^2}{r^2 - N^2}. \end{aligned} \tag{4.5}$$

For the comoving observer of Cooperstock and Tieu, who would be seen as stationary if viewed from infinity, $\Omega = 0$. We then have

$$v = -\omega e^{\psi-\eta} = \frac{N}{r^2 - N^2}\frac{\sqrt{r^2 - N^2}\sqrt{r^2 - N^2}}{r} = \frac{N}{r}, \tag{4.6}$$

and thus the observed tangential velocity is $V = \frac{N}{r}$ for all $r > N$ not only for $r \gg N$.

4.1.3 The Region $r < N$

One can see that values of the coordinate $r < N$ result in superluminal velocities. However, the metric may also be written

$$ds^2 = \frac{-r^2dt^2}{r^2 - N^2} + (r^2 - N^2)\left(d\phi + \frac{Ndt}{r^2 - N^2}\right)^2 + e^{\nu}(dz^2 + dr^2).$$

We can see that the length of the axial Killing vector $g_{\phi\phi} = r^2 - N^2$ pinches off at $r = N$. Furthermore, at $r < N$ ϕ becomes a *timelike* direction and t becomes spacelike. The surface $r = N$ would appear to be nonsingular as long as the undetermined metric functions are well behaved, since $\det g_{\mu\nu}$ is finite then. However, we could have an isotropic crushing singularity if $e^{\nu} \to 0$, i.e., $\nu \to -\infty$. In this case space pinches off equally in all directions.

Whether or not the surface is a physical singularity may depend on the matter distribution $\rho(r, z)$. An alternative to a physical singularity is suggested by the similarity of the $r = N$ surface to the horizon $r = r_s$ in the Schwarzschild metric,

$$d\tau^2 = \left(1 - \frac{r_s}{r}\right)dt^2 - \left(1 - \frac{r_s}{r}\right)^{-1}dr^2 - r^2\left(d\theta^2 + \sin^2\theta\, d\phi^2\right).$$

But in the Schwarzschild case the horizon is a coordinate singularity and it is the Killing vector g_{tt} that pinches off instead. It may be possible to reverse the roles of t and ϕ in the region $r < N$ by choosing $U^{\mu} = \delta^{\mu}_{\phi}$ but this is not within the scope of this project. Related issues have been discussed in [27].

In any case, the metric of Cooperstock and Tieu and Balasin and Grumiller cannot be interpreted as a galactic model for any values of $r \leq N$. Cooperstock and Tieu do not address this region in [14], and Balasin and Grumiller choose to "cut out the domains where $N(r,z) \gtrsim r$ and blithely ignore them". However, they had previously mentioned that their general form of $N(r,z)$ has to be constrained by setting some boundary condition such as requiring certain behaviour of N as $r \to 0$. This is not true as if we are to remove the region $r \leq N$ then we should not be setting any boundary conditions there and so we cannot set a boundary condition at $r = 0$.

Since the coordinate surface $r = N$ corresponds to the pinching off of the axial Killing vector it could either correspond to the physical centre of the galaxy or some finite surface, such as an horizon associated with a central black holes. In either case, it represents a physical boundary on the spacetime and appropriate boundary conditions ($\rho = 0$ or $\rho \to \infty$) should be set there.

4.2 Towards a General Solution for Prescribed Dust

Both of the models have assumed that the form of $N(r,z)$ is separable. However, this assumption may be incorrect and we believe that some inquiry should be made into whether one can obtain a more general form of $N(r,z)$. It may be possible to make some empirically based assumptions about the density profile and try to solve Einstein's equations directly.

In the following we investigate this possibility.

4.2.1 Discrete Sums and Integral Transforms

In [14] the authors use a discrete sum of solutions to the Einstein field equations which form an orthogonal basis. They do not appear to have considered using an integral transform method such as [17] uses. The orthogonal basis method gives an approximation, and if one has good basis functions, only a few terms should be needed to achieve a very good approximation. In such cases, this method therefore has the advantages that it is mathematically easier to set boundary conditions and find the coefficients in the sum. However, using the integral form as in [17] can give an exact solution.

Balasin and Grumiller evaluate the integral of their form of $N(r,z)$ by observing that

$$\int_0^\infty dx x K_1(x) \cos\left(\frac{ax}{r}\right) = \frac{\pi}{2} \frac{r^3}{(a^2+r^2)^{3/2}}, \tag{4.7}$$

where $x = \lambda r$ and the integral is from $\lambda = 0$ to ∞ with r held constant. We observe that

$$\int_0^\infty dx x J_1(x) \exp\left(\frac{ax}{r}\right) = \frac{r^3}{(a^2+r^2)^{3/2}}, \tag{4.8}$$

so that, given boundary conditions, solutions could be obtained using Cooperstock and Tieu's choice of N in a way analogous to the methods in [17]. However, we point out that the use of $N(0, z \geq 0) = \frac{2}{\pi} \int_0^\infty d\lambda \cos(\lambda z) \int_0^\infty dx C(x) \cos(\lambda x)$ is essentially meaningless as the model is not defined for values of $r < N$.

It is worth noting here the reason Balasin and Grumiller rejected the nonsmooth CT solution. There is a discontinuity in the derivative of the density at $z = 0$, so one must apply matching conditions, which in GR follows the formalism of Israel junction conditions. The weak energy condition stipulates that for every future-pointing timelike vector field $\vec{X}$, the matter density observed by the corresponding observers is always nonnegative:

$$\rho = T_{\mu\nu} X^\mu X^\nu \geq 0, \tag{4.9}$$

where ρ is the mass density, and $T_{\mu\nu}$ is the energy momentum tensor. At $z = 0$ Balasin and Grumiller obtain $\rho = -P$, where P is the pressure. Thus since $\rho \neq 0$ they find that such a source violates the weak energy condition, or one has negative pressure. In either case one has exotic matter. Moreover, a key assumption in obtaining the metric (2.1), absence of pressure, is violated.

4.2.2 General Solution

The Einstein field equations contain some redundancy on account of the Bianchi identities. Presumably some of the second order equations follow as consequences of the first order equations (2.9) and (2.10). Here we check this:

$$\frac{\partial}{\partial r}(2.9) \implies \nu_r + r\nu_{rr} + N_r N_{rr} - N_z N_{rz} = 0, \tag{1a}$$

$$\frac{\partial}{\partial z}(2.9) \implies r\nu_{rz} + N_r N_{rz} - N_z N_{zz} = 0, \tag{1b}$$

$$\frac{\partial}{\partial r}(2.10) \implies \nu_z + r\nu_{zr} + N_z N_{rr} + N_r N_{zr} = 0, \tag{2a}$$

$$\frac{\partial}{\partial z}(2.10) \implies r\nu_{zz} + N_z N_{rz} + N_r N_{zz} = 0, \tag{2b}$$

$$(2a) - (1b) \implies \nu_z + N_z N_{rz} + N_r N_{zz} = 0.$$

$$\implies N_z\{N_{rr} + N_{zz} - \frac{N_r}{r}\} = 0, \qquad \text{as } \nu_z = -\frac{N_r N_z}{r} \text{ by (2.10)},$$

$$\implies N_z = 0 \text{ or } N_{rr} + N_{zz} - \frac{N_r}{r} = 0,$$

and equation (2.12) is a dependent equation as expected. Taking (1a)+(2b) gives us

$$r(\nu_{rr} + \nu_{zz}) + \nu_r + N_r(N_{rr} + N_{rr}) = 0.$$

And then by (2.9) and (2.12),

$$r^2(\nu_{rr} + \nu_{zz}) + \frac{1}{2}({N_r}^2 + {N_z}^2) = 0.$$

Hence (2.11) is a dependent equation, and thus (2.11) and (2.12) are indeed fully contained in (2.9) and (2.10).

The independent equations are (2.9), (2.10) and (2.13), a system of three 1st order nonlinear PDEs.

$$\left.\begin{array}{ll} (2.13) & {N_r}^2 + {N_z}^2 = 8\pi G\rho r^2 e^\nu \\ (2.9) & {N_z}^2 - {N_r}^2 = 2r\nu_r \end{array}\right\} \implies \begin{array}{l} 4\pi G\rho r^2 e^\nu + r\nu_r = {N_z}^2 \\ 4\pi G\rho r^2 e^\nu - r\nu_r = {N_r}^2. \end{array}$$

And so we obtain

$$N_r = \pm\sqrt{4\pi G\rho r^2 e^\nu - r\nu_r}, \tag{4.10}$$

$$N_z = \pm\sqrt{4\pi G\rho r^2 e^\nu + r\nu_r}. \tag{4.11}$$

From (2.12),

$$\nu_r^2 + \nu_z^2 = 16\pi^2 G^2\rho^2 e^{2\nu} r^2 = \kappa^2\mu^2 r^2, \tag{4.12}$$

or alternatively,

$$u_r^2 + u_z^2 = 16\pi^2 G^2\rho^2 r^2 = \kappa^2\rho^2 r^2, \tag{4.13}$$

where $\mu = \rho e^\nu$, $u = e^{-\nu}$ and $\kappa^2 = 16\pi^2 G^2$.

If ρ is a prescribed function then we have a simple first order PDE, quadratic in derivatives, of two variables. It is possible that general techniques might be applied. In applying such techniques careful attention must be paid to boundary conditions.

4.2.3 Prescribing an Asymptotic Density Profile

Here we investigate whether prescribing the empirical density profile $\mu \propto \exp(-r/H)\exp(-z/h)$ makes sense in these DEs in the asymptotic limit. Let us define F as

$$F = \nu_r^2 + \nu_z^2 - \kappa^2\mu^2 r^2 = 0, \tag{4.14}$$

Then the PDE (4.12) is equivalent to five ODEs:

$$\frac{dr}{d\lambda} = F_{\nu_r} = 2\nu_r, \tag{4.15}$$
$$\frac{dz}{d\lambda} = F_{\nu_z} = 2\nu_z, \tag{4.16}$$
$$\frac{d\nu}{d\lambda} = \nu_r\frac{dr}{d\lambda} + \nu_z\frac{dz}{d\lambda} = 2(\nu_r^2 + \nu_z^2), \tag{4.17}$$
$$\frac{d\nu_r}{d\lambda} = F_r = 2\kappa^2\left(\mu_r\mu r^2 + \mu^2 r\right), \tag{4.18}$$
$$\frac{d\nu_z}{d\lambda} = F_z = 2\kappa^2\left(\mu_z\mu r^2\right). \tag{4.19}$$

Thus, keeping only leading order terms in r, and using $\mu_r \propto -\frac{1}{H}\mu$,

$$\begin{aligned}\frac{d\nu_r}{d\lambda} &= 2\kappa^2\left(\mu_r\mu r^2 + \mu^2 r\right)\\ &\sim \frac{-2\kappa^2 r^2}{H}\exp\left(\frac{-2r}{H}\right),\end{aligned} \tag{4.20}$$
$$\frac{dr}{d\lambda} = 2\nu_r, \tag{4.21}$$
$$\implies \frac{d\nu_r}{dr} \sim \frac{-\kappa^2 r^2}{2H\nu_r}\exp\left(\frac{-2r}{H}\right). \tag{4.22}$$

Rearranging and integrating, keeping only leading order terms,

$$\int \nu_r d\nu_r \sim \frac{-\kappa^2}{2H}\int r^2\exp\left(\frac{-2r}{H}\right)dr, \tag{4.23}$$
$$\implies \nu \sim \frac{\pm H\kappa}{2} r\exp\left(\frac{-r}{H}\right) \tag{4.24}$$
$$\to 0 \text{ as r} \to \infty, \text{ as required.}$$

Similarly, keeping only leading order terms in z, and using $\mu_r \propto -\frac{1}{h}\mu$,

$$\begin{aligned}\frac{d\nu_z}{d\lambda} &= 2\kappa\mu_z\mu r^2\\ &\sim \frac{-2\kappa^2}{h}\exp\left(\frac{-2z}{h}\right),\end{aligned} \tag{4.25}$$
$$\frac{dz}{d\lambda} = 2\nu_z, \tag{4.26}$$
$$\implies \frac{d\nu_z}{dz} \sim \frac{-\kappa^2}{2h\nu_z}\exp\left(\frac{-2z}{h}\right). \tag{4.27}$$

Rearranging and integrating, keeping only leading order terms,

$$\int \nu_z d\nu_z \sim \frac{-\kappa^2}{2h}\int \exp\left(\frac{-2z}{h}\right)dz, \tag{4.28}$$
$$\implies \nu \sim \frac{\pm h\kappa}{2}\exp\left(\frac{-z}{h}\right) \tag{4.29}$$
$$\to 0 \text{ as z} \to \infty, \text{ as required.}$$

It therefore appears that one can indeed have μ proportional to the empirically observed asymptotic density profile $\mu \propto \rho \propto \exp(-r/H)\exp(-z/h)$ in the asymptotic limit. This means that were we to try solving (4.12) directly, setting the density profile at spatial infinity equal to such an observed profile would be viable. It is then interesting that the two solutions to Einstein's equations with the ansatz that $N(r,z)$ is separable did not exhibit such asymptotic behaviour, and perhaps suggests that the ansatz need not hold.

4.2.4 The Separation Ansatz

Setting boundary conditions on $r = N$ appears to be incompatible with the assumption of separability since the derivatives of N viz. $N_r = 1$, $N_z = 0$ give contradictions when substituted into Einstein's equations. As we concede that this problem may be limited only to a region near the centre of a galaxy, we proceed to examine further the implications of the separation ansatz in the Einstein field equations.

Let us now analyse the implications of substituting $N(r,z) = R(r)Z(z)$ into Einstein's equations. From (2.10) we have

$$\begin{aligned} \nu_z &= -\frac{R\frac{dR}{dr}Z\frac{dZ}{dz}}{r} \\ \implies \nu &= -\frac{1}{2}\frac{R\frac{dR}{dr}}{r}Z^2. \end{aligned} \tag{4.30}$$

Therefore if N is separable, so is ν; let $\nu = f(r)g(z)$. Equation (2.13) gives

$$8\pi G\rho e^{\nu} = \frac{\frac{dR}{dr}^2 Z^2 + R^2\frac{dZ}{dz}^2}{r^2}. \tag{4.31}$$

The two possible forms of $Z(z)$ when N is separable were $Z = e^{-k|z|}$, for which $\frac{dZ}{dz}^2 = k^2Z^2$, and $Z = \cos(kz)$, for which $\frac{dZ}{dz}^2 = 1 - Z^2$.

In the former case we would have

$$8\pi G\rho e^{f(r)g(z)} = Z^2\frac{(\frac{dR}{dr}^2 + k^2R^2)}{r^2}, \tag{4.32}$$

where the right hand side is separable, while the left hand side is not, unless $\rho = h(r,z)e^{-f(r)g(z)}$ for some separable function h.

When $Z = \cos(kz)$ we would have, from (4.31),

$$8\pi G\rho e^{f(r)g(z)} = Z^2\frac{(\frac{dR}{dr}^2 - R^2)}{r^2} + \frac{R^2}{r^2}. \tag{4.33}$$

Asymptotically we have $e^{\nu} \to 1$. The empirically observed density used in Section 3.2.1 gives

$$8\pi G\rho = Z^2\frac{(\frac{dR}{dr}^2 - R^2)}{r^2} + \frac{R^2}{r^2} \propto \exp(-r/H)\exp(-z/h). \tag{4.34}$$

Here the right hand side is separable and the left hand side is not. Therefore by assuming a separable $N(r,z)$ one cannot obtain the empirically observed density profile in the asymptotic limit.

From this we gather that the separability of $N(r,z)$ is not an acceptable ansatz, or at the very least that the Cooperstock and Tieu solution cannot be made consistent with the empirically observed density profile and a flat space metric ($e^{\nu} = 1$) at spatial infinity. So it appears we will have to try to solve the PDE obtained in Section 4.2.2. If this cannot be done by using general techniques, one would have to use numerical integration to obtain a solution.

Chapter 5

Conclusion

In this project we have analysed and extended the models of Cooperstock and Tieu and Balasin and Grumiller which attempt to use a cylindrically symmetric, stationary rotating dust solution in general relativity alone to model spiral galaxies. Cooperstock and Tieu use a linear superposition of (nonsmooth) solutions of the Einstein field equations to do this, while Balasin and Grumiller take an integral over all possible modes of the smooth solutions to the Einstein equations, and impose boundary conditions. A major assumption of both models is that the function, $N(r, z)$, found in the metric, which relates to both the density and rotation velocity of matter in the galaxy, is separable.

We have confirmed that, assuming separability in the radial and azimuthal directions, one can use an orthogonal basis of solutions to the Einstein field equations to fit to the velocity of spiral galaxies. However, this does not give information about the predictive power of the model. For that one must compare the calculated density to observation, a test which the CT model has failed in the instance of the Milky Way galaxy.

Since the model is undefined for $r \leq N$, the question also arises whether Cooperstock and Tieu's assumption, that one must have $V = 0$ at $r = 0$, which excluded the use of Bessel functions of the second kind, Y_1, in addition to J_1, was justified.

It was found that in the CT model the density decayed as r^{-1} far from the galactic centre in the r direction, not nearly as quickly as the empirically found exponential decay. In addition, the metric in this model does not approach that of flat space at spatial infinity. These problems cannot be remedied by using Bessel functions of the second, rather than first, kind.

The BG model fared better, its metric matching that of flat space at infinity and with an asymptotic density decay of r^{-4} and z^{-4} in the r and z directions, respectively. However, this decay was a result of the imposition of unsuitable boundary conditions set in the area $r \leq N$, a region where the metric is not defined in these models.

We showed that Cooperstock and Tieu could have used the continuous integral approach with their solution. However, we have not attempted to do so, as it was found that this solution cannot be made consistent with the empirically observed density profile and a flat space metric at spatial infinity, even though this can be done for the Einstein field equations obtained from the metric in both models. In addition, Balasin and Grumiller have observed that the CT solution, due to not being smooth, either violates the weak energy condition or has negative pressure at $z = 0$, yielding nonbaryonic matter and violating the model's assumption of no pressure. This, along with the results of [24] showing that the CT model predicts interior densities lower than observed in the Milky Way, lead us to believe that the solution of Cooperstock and Tieu is not a viable one.

Having found that the boundary conditions used to calculate rotation velocity in the BG model are not appropriate, new boundary conditions must first be set before one could proceed with this model. In attempting to do this we discovered apparent contradictions in the assumption of a separable form for the rotation velocity.

We believe that one should attempt to solve the Einstein field equations more generally, which may involve numerical integration. In doing so one would have to be careful to set physically appropriate boundary conditions at the surface $r = N$, which is the true boundary of the physically allowed region. This falls outside the scope of the present project.

If these solutions were to be found successfully, it would be an important ingredient for understanding our current cosmological models. It might give an indication of what fraction of the total mass of the universe (or at least, the mass of spiral galaxies) was dark matter, thus providing evidence to verify or disprove models such as ΛCDM, which predicts a dark matter to baryon ratio of 4.9:1, the timescape model, which currently predicts a ratio of 2-5:1 (typically 3:1 as a best fit), or Modified Newtonian Dynamics, which abandons Cold Dark Matter entirely. In addition, it could give a more accurate picture of the distribution of dark matter.

Acknowledgements

Many thanks to Assoc. Prof. David Wiltshire for his teaching, counsel and inspiration, and for providing excellent lecture notes. I also thank Dr. Teppo Mattsson for answering my questions and some stimulating discussions.

Thank you to Steven Tieu for providing us with the rotation curve data used. Also to Rick Hessman for his comparison of calculated and observed surface brightnesses of the Milky Way.

I was lucky to share the company of many capable peers and I thank in particular Kane O'Donnell, Hayden Lee and past student Will Frost for their help and advice.

Thank you to the New Zealand Federation of University Women (Inc.) Canterbury Branch for their financial support.

Lastly a big thanks to my partner Dr. Michael Langton for getting me started with programming, his computer expertise and continual support.

Bibliography

[1] S. van den Bergh, Publ. Astron. Soc. Pac. **111**, 657 (1999).

[2] P. Tisserand *et al.*, Astron. Astrophys. **469**, 387 (2007).

[3] D. Graff and K. Freese, Astrophys. J. **456**, L49 (1996).

[4] G. Najita, J. Tiede and S. Carr, Astrophys. J. **541**, 977 (2000).

[5] J. Silk, *The Big Bang* (Freeman, San Francisco, 1989).

[6] R. Bernabei *et al.*, Eur. Phys. J. **C67**, 39 (2010).

[7] D. Clowe *et al.*, Astrophys. J. **648**, L109 (2006).

[8] E. Komatsu *et al.*, Astrophys. J. Suppl. **192**, 18 (2011).

[9] D. L. Wiltshire, New J. Phys. **9**, 377 (2007).

[10] B. M. Leith, S. C. C. Ng, and D. L. Wiltshire, Astrophys. J. **672**, L91 (2008).

[11] D. L. Wiltshire, Phys. Rev. **D80**, 123512 (2009).

[12] M. S. Turner, Proc. Astron. Soc. Pacific **111**, 264 (1999).

[13] F. Rahaman, K. Nandi, A. Bhadra, M. Kalam, and K. Chakraborty, Phys. Lett. **B694**, 10 (2010).

[14] F. Cooperstock and S. Tieu, Int. J. Mod. Phys. **A22**, 2293 (2007).

[15] J. Magorrian *et al.*, Astron. J. **115**, 2285 (1998).

[16] P. S. Negi, Grav. Cosmol. **9**, 291 (2003).

[17] H. Balasin and D. Grumiller, Int. J. Mod. Phys. **D17**, 475 (2008).

[18] W. J. van Stockum, Proc. R. Soc. Edin. **57**, 135 (1937).

[19] S. Tieu, Private communication.

[20] G. Gentile, B. Famaey, and W. J. G. de Blok, Astron. Astrophys. **527**, A76 (2010).

[21] W. J. G. de Blok *et al.*, Astron. J. **136**, 2563 (2008).

[22] F. Hessman, Private communication.

[23] R. A. Swaters, R. H. Sanders, and S. S. McGaugh, Astrophys. J. **718**, 380 (2010).

[24] B. Fuchs and S. Phelps, New Astron. **11**, 608 (2006).

[25] P. Cuddeford, Mon. Not. Roy. Astron. Soc. **262**, 1076 (1993).

[26] J. M. Bardeen, Astrophys. J. **162**, 71 (1970).

[27] T. Zingg, A. Aster, and D. Trautmann, Adv. Stud. Theor. Phys. **1**, 409 (2007).

Appendix A

Details of Velocity Fit Comparison

Galaxy	10 parameters	5 parameters	Iso free	Iso Kroupa	Iso Salpeter	NFW free	NFW Kroupa	NFW Salpeter	MOND free	MOND SSM	MOND GFdB
NGC3031	0.1500	0.3849	3.2683	3.8809	3.9351	3.3068	3.6150	4.3607	3.6726	4.0403	4.3808
NGC3198	0.2576	1.5422	0.3630	1.4165	2.1541	0.3694	2.0594	2.8798	1.1119	3.9815	6.0290
NGC7331	0.1141	0.9704	0.2598	0.3066	2.9295	0.2389	3.6150	4.3607	0.2627	0.2903	0.3113
ddo154	0.1201	0.2068	0.2772	0.4362	0.4390	0.2772	0.8267	0.8219	0.3551	3.6726	3.8227
ic2574	0.1239	0.1416	0.1622	0.1657	0.1742	1.6494	1.7308	1.8107	1.0096	2.5115	4.3106
NGC925	0.0374	0.1401	0.6831	1.1392	2.1511	1.1154	2.1712	2.8129	2.0796	2.7407	2.5020
NGC2403	0.7610	3.4644	0.4992	0.9698	0.7885	0.5524	0.5744	0.5579	0.5383	4.2825	2.6513
NGC2841	0.5795	7.5353	0.1821	0.2151	0.2722	0.1901	0.2277	0.4192	0.3610	4.9049	2.6280
NGC2903	0.2187	1.4750	0.3554	3.7508	0.6300	0.2450	0.4134	0.3556	0.8942	1.9845	1.1608
NGC2976	0.0803	0.4347	0.5105	0.4959	1.7581	1.6535	1.9072	2.7760	0.6803	1.8326	1.7468
NGC3521	1.0680	3.3821	4.0456	4.7590	8.0771	5.4818	5.5555	8.5281	6.2367	6.3002	6.3032
NGC4736	1.2883	10.5654	1.5279	1.7369	1.5221	1.4353	NA	1.5116	1.6929	4.9065	6.1881
NGC5055	7.5466	26.4101	0.8662	1.0329	8.1391	0.5669	1.4757	10.3022	0.9469	1.4028	2.3869
NGC6946	0.5830	3.0292	0.9634	0.9814	1.4524	1.0066	1.0355	2.5894	1.0270	3.6726	1.0794
NGC7793	0.3841	2.9082	2.8303	3.5658	2.9706	3.5166	3.7485	4.1728	3.1041	7.9739	6.4630

Table A.1: Reduced χ^2s for fits to the rotation curves of 15 spiral galaxies used in Section 2.3. This compares the fits of the CT model with 5 and 10 parameters; the Nevaro-Frenk-White and isothermal halo models with a mass-to-light ratio derived from either a Kroupa or a Salpeter initial mass function or as a free parameter; and MOND,with the MOND acceleration parameter of $a_0 = 1.0 \times 10^{-8}$cm s^{-2}, $a_0 = 1.22 \times 10^{-8}$cm s^{-2} or a_0 as a free parameter.

Appendix B

Python Code

bessel_plotter.py

```
import scipy
import scipy.linalg
import scipy.special
import pylab
from scipy.special import j0, j1, jn
import scipy.optimize
import scipy.stats
import matplotlib
import matplotlib.pyplot
import data  #grabs THINGS rotation curve data from data.py

g=1       #which galaxy to plot
param=10 #number of terms in the sum

class Approx:
    '''does a least squares fit'''
    def __init__(self, galaxy, r0=None, param=param):
        self.galaxy = galaxy
        self.r0 = galaxy.r0opt[param] if r0 == None else r0
        self.k = scipy.special.jn_zeros(0, param)/self.r0
        self.approx()

    def approx(self):
        A = scipy.empty((len(self.galaxy.x), len(self.k)))
        for i in xrange(len(self.galaxy.x)):
            for j in xrange(len(self.k)):
                A[i, j] = j1(self.k[j]*self.galaxy.x[i])
        self.mkC = scipy.linalg.lstsq(A, self.galaxy.y)[0]/3e8

    def eval(self, x0):
        '''calculates velocities at given values of r'''
        v = 3e8*self.mkC[:,scipy.newaxis]*j1(self.k[:,scipy.newaxis]*x0)
        return v.sum(0)

    def chi2(self):
        '''calculates the chi^2'''
        return scipy.stats.chisquare(self.eval(self.galaxy.x),
                                     self.galaxy.y)[0]

    def chi2err(self):
        '''calculates the chi^2 with error bars accounted for'''
        return ((self.eval(self.galaxy.x)-self.galaxy.y)**2
                /self.galaxy.err**2).sum(0)

class Chi2Approx(Approx):
```

```
    '''does a chi^2 miminimising fit'''
    def __init__(self, galaxy, r0=None, param=param):
        Approx.__init__(self, galaxy, r0, param)

    def approx(self):
        A = scipy.empty((len(self.galaxy.x), len(self.k)))
        for i in xrange(len(self.galaxy.x)):
            for j in xrange(len(self.k)):
                A[i, j] = j1(self.k[j]*self.galaxy.x[i])
        for i in xrange(len(self.galaxy.x)):
            A[i,:] *= 1/self.galaxy.y[i]
        self.mkC = scipy.linalg.lstsq(A, scipy.ones(len(self.galaxy.y)))[0]/3e8

class ApproxCT(Approx):
    '''produces the fit of CT for comparison on the plot'''
    def __init__(self, galaxy, r0=None, param=param):
        Approx.__init__(self, galaxy, r0, param)

    def approx(self):
        self.mkC = self.galaxy.mkc_ct

class ApproxChi2Err(Approx):
    '''does chi^2 minimised fit, with uncertainties'''
    def __init__(self, galaxy, r0=None, param=param):
        Approx.__init__(self, galaxy, r0, param)

    def approx(self):
        A = scipy.empty((len(self.galaxy.x), len(self.k)))
        for i in xrange(len(self.galaxy.x)):
            for j in xrange(len(self.k)):
                A[i, j] = j1(self.k[j]*self.galaxy.x[i])
        y1 = self.galaxy.y.copy()
        for i in xrange(len(self.galaxy.x)):
            A[i,:] *= 1/(self.galaxy.err[i])**2
            y1[i] = self.galaxy.y[i]/(self.galaxy.err[i])**2
        self.mkC = scipy.linalg.lstsq(A, y1)[0]/3e8

def chi2err(r0, galaxy, param):
    '''calculates the chi^2 with uncertainties'''
    if r0 <= 0:
        return 1e10
    approxchierr = ApproxChi2Err(galaxy, r0, param)
    return approxchierr.chi2err()

def r0min(galaxy, param=param):
    '''optimizes the value of r0'''
    r0s = scipy.linspace(1, 51, 25)
    startpts = scipy.array([chi2err(r0, galaxy, param) for r0 in r0s])
    r = r0s[startpts.argmin()]
    minn = scipy.optimize.fmin(chi2err, r, (galaxy,param),xtol=1e-14,
                               ftol=1e-14, full_output=1, disp=0)
    return minn[0], minn[1] #returns the optimal r0 and its chi^2

def makeplot(g,param=10, show=False):
    '''plots the fit, default of 10 terms, to be called by a script which
    saves plots for all galaxies'''
    galaxies = data.galaxies_things
    r0 = galaxies[g].r0opt          #optimal r0
    rf= galaxies[g].rf              #largest r value to plot
    mkc_ct = galaxies[g].mkc_ct     #values of -k_n*C_n  in CT paper
    x0 = scipy.linspace(0,rf,200) #creates an array of r values to plot
    approx = Approx(galaxies[g])
    approxct = ApproxCT(galaxies[g])
```

```
    approxchi = Chi2Approx(galaxies[g])
    if not scipy.isnan(galaxies[g].err[0]): #calculates the chi^2 with
        #uncertainties accounted for except for the Milky Way
        approxchierr = ApproxChi2Err(galaxies[g])
    vm = approx.eval(x0)      #creates velocity data for a least squares fit
#     vct = approxct.eval(x0) #creates velocity data for the CT coefficients
    v = approxchi.eval(x0)   #creates velocity data for a chi^2 minimised fit
    if not scipy.isnan(galaxies[g].err[0]):
        verr= approxchierr.eval(x0) #creates velocity data for a chi^2 with
            #uncertainties fit if the galaxy is not the Milky Way
    print 'my least squares fit:'
#     print '['+', '.join(['%.16g'%e for e in approx.mkC])+']'
    print 'chi^2=', approx.chi2()
    print 'chi^2 with error bars=', approx.chi2err()
    print 'chi^2/dof=', approx.chi2err()/(len(galaxies[g].x)-(param+1))
#     print "CT's coeffs:"
#     print '['+', '.join(['%.16g'%e for e in mkc_ct])+']'
#     print 'chi^2=', approxct.chi2()
    print 'Chi^2 minimised fit'
#     print '['+', '.join(['%.16g'%e for e in approxchi.mkC])+']'
    print 'chi^2=', approxchi.chi2()
    print 'chi^2 with error bars=', approxchi.chi2err()
    print 'chi^2/dof=', approxchi.chi2err()/(len(galaxies[g].x)-(param+1))
    print 'Chi^2 minimised with error fit , coeffs:'
    if not scipy.isnan(galaxies[g].err[0]):
        print '['+', '.join(['%.16g'%e for e in approxchierr.mkC])+']'
        print 'chi^2=', approxchierr.chi2err()
        rchi = approxchierr.chi2err()/(len(galaxies[g].x)-(param+1))
        print data.galaxynames[g], 'C&T model (',param, 'parameters)'\
        'chi^2/dof=',rchi
    minn = r0min(galaxies[g])
    print 'Optimal r0=%.16g' % minn[0], 'chi^2 at this r0=%.16g' % minn[1]
    pylab.plot(approx.galaxy.x,approx.galaxy.y/1000,'x', color='b',
               label='datapts')
#     pylab.plot(x0,v, 'm', label='chi^2 minimised')
#     pylab.plot(x0, vct, 'g', label='ct') #plots Cooperstock and Tieu's fit
    if not scipy.isnan(galaxies[g].err[0]):
        pylab.plot(x0, verr/1000,'r',label='$\chi^2$ minimised fit w/error')
        matplotlib.pyplot.errorbar(galaxies[g].x, galaxies[g].y/1000,
        galaxies[g].err/1000, fmt=None, ecolor='c')
#creates error bars except in the case of the Milky Way for which the errors
#are "nan" as the Milky Way is not in the THINGS dataset so we don't have
#uncertainty information for it.
    b, d=max(approx.galaxy.x), max(approx.galaxy.y/1000)
    e=max(galaxies[g].err/1000)
    pylab.axis([0, b+0.2, 0, d+e])  #sets appropriate axes
    pylab.xlabel('r in Kpc')
    pylab.ylabel('V in kms$^{-1}$')
    pylab.title(data.galaxynames[g]+
                ' velocity curve fit(%d parameters)'%param)
    pylab.legend(title = '$\chi^2$/d.o.f. = %.6g' %rchi, loc=4)
    matplotlib.pyplot.annotate( #adds galaxy name inside the plot
        data.galaxynames[g], xy=(300,88), xycoords='axes points', size=18)
    pylab.gcf().set_size_inches((8.4, 5.6))  #size of image to output
    if show:
        pylab.show()

if __name__ == '__main__':     #for plotting and displaying individual
    makeplot(g,param, True)    #galaxies with this program
```

data.py

```
import scipy
```

```
import scipy.linalg
import scipy.special
import pylab

x = {#rotation curve data provided by Steven Tieu, radii
  'Milky Way':
      scipy.array([3.02521008, 3.52941176, 4.15966387, 5.86134454, 6.61764706,
                   7.24789916, 8.19327731, 8.82352941, 9.51680672,
                   10.02100840, 10.46218487, 11.09243697, 11.72268908,
                   12.66806723, 13.29831933, 14.24369748, 15.18907563,
                   15.81932773, 16.76470588, 17.39495798, 18.34033613,
                   18.97058824, 19.78991597, 20.42016807, 21.36554622,
                   21.99579832, 22.94117647, 23.57142857, 24.51680672,
                   25.14705882, 26.09243697, 27.03781513, 27.66806723,
                   28.61344538, 29.24369748]),
  'NGC3031':
      scipy.array([3.434, 3.703, 3.939, 4.208, 4.444, 4.713, 4.949, 5.218,
                   5.454, 5.723, 5.959, 6.161, 6.464, 6.700, 6.969, 7.205,
                   7.441, 7.744, 7.979, 8.215, 8.451, 8.686, 8.922, 9.259,
                   9.461, 9.696, 9.966, 10.20, 10.47, 10.70, 10.97, 11.21,
                   11.48, 11.71, 11.95, 12.22, 12.49, 12.72, 12.99, 13.23,
                   13.46, 13.70, 13.97, 14.24, 14.47, 14.74, 14.98, 15.25,
                   15.48, 15.75, 16.02, 16.22, 16.46, 16.76, 17.00, 17.23,
                   17.50, 17.74, 18.01, 18.24, 18.51, 18.78, 19.02, 19.29,
                   19.56, 19.79, 20.03, 20.26, 20.53, 20.80, 21.04 ]),
  'NGC3198':
      scipy.array([1.54329, 2.1496, 2.81102, 3.47246, 4.07873, 4.74015,
                   5.40158, 6.06298, 6.77954, 7.38584, 8.04723, 9.42519,
                   10.8031, 12.126, 13.4488, 14.8268, 16.1496, 17.4725,
                   18.7953, 20.1181, 21.3858, 22.7087, 23.9764, 25.2992,
                   26.6221, 27.8897, 29.2126 ]),
  'NGC7331':
      scipy.array([3.32488, 4.41624, 5.5076, 6.5736, 7.66496, 8.7056, 9.82232,
                   10.8883, 11.9797, 13.0457, 14.1117, 15.203, 16.269, 17.3604,
                   18.4264, 19.4924, 20.5838, 21.6751, 22.7411, 23.8325,
                   24.8985, 25.9645, 27.0558, 28.1472, 29.2132, 30.2792,
                   31.3706, 32.4619, 33.5279, 34.6193, 35.6853, 36.7766]),
    }

y = {           #rotation curve data provided by Steven Tieu,
  'Milky Way':  #velocities corresponding to the above radii
    scipy.array([209859.15493, 211971.83099, 214084.50704, 220422.53521,
                 222535.21127, 223943.66197, 224647.88732, 225352.11268,
                 226056.33803, 226056.33803, 226056.33803, 226056.33803,
                 225352.11268, 225352.11268, 224647.88732, 223943.66197,
                 223239.43662, 222535.21127, 221830.98592, 221126.76056,
                 220422.53521, 219718.30986, 219014.08451, 218309.85915,
                 217605.63380, 216901.40845, 216197.18310, 215492.95775,
                 214788.73239, 214084.50704, 213380.28169, 212676.05634,
                 212676.05634, 211971.83099, 211971.83099]),
  'NGC3031':
    scipy.array([222013, 224004, 223340, 226991, 231637, 234955, 230973, 235951,
                 237942, 240929, 243252, 244247, 245575, 243252, 241592, 238938,
                 237942, 235951, 231969, 230973, 227986, 225000, 223008, 219358,
                 216371, 214380, 210730, 207411, 203097, 199778, 198451, 197455,
                 196128, 195796, 194469, 195464, 192477, 192809, 187831, 187168,
                 189159, 188495, 186504, 184513, 184845, 185508, 186172, 178207,
                 177876, 178539, 174889, 180530, 178207, 178539, 177212, 174225,
                 178539, 176548, 176548, 177212, 179867, 178207, 175884, 169579,
                 169247, 173230, 173893, 171570, 169247, 169579, 168252]),
  'NGC3198':
    scipy.array([91823.8, 110273, 122851, 132495, 141300, 145073, 147170,
                 147589, 151363, 154298, 155556, 156394, 152621, 152621,
```

```
                153459, 152621, 149686, 148847, 148008, 145912, 146751,
                48008, 148008, 148847, 150105, 150105, 149266]),
  'NGC7331':
    scipy.array([260237, 255193, 25638, 25638, 25638, 254303, 247181, 246291,
                245401, 243323, 241543, 237389, 235312, 232344, 233531,
                235312, 236498, 237389, 239466, 237389, 236498, 235312,
                237389, 238279, 238279, 240356, 235608, 235312, 238279,
                236498, 240356, 237389]),
    }

mkc_ct = {'Milky Way': #values of -k_n*C_n in Cooperstock and Tieu 2006
       scipy.array([0.0012636497740, 0.0004520156256, 0.0001785404942,
                    0.0002946610499, 0.0000103378815, 0.0002127633340,
                    -0.0000221015927, 0.0001346275993, -0.0000123824930,
                    0.0000666973093]),
      'NGC3031':
        scipy.array([0.0011694103480, 0.0004356556836, 0.0003677376760,
                     0.0001484103801, 8.37048346e-05, 4.14084713e-05,
                     4.29277032e-05, 5.50130755e-05, 2.38560073e-05,
                     1.29841761e-05]),
      'NGC3198':
        scipy.array([0.00093352334660, 0.00020761839560, 0.00022878035710,
                     9.325578799e-05, 0.00007945062639, 0.00006081834319,
                     0.00003242780880, 3.006457058e-05, 1.687931928e-05,
                     3.651365350e-05]),
      'NGC7331':
        scipy.array([0.0015071991080, 0.0003090462519, 0.0003960391396,
                     0.0001912008955, 0.0002161444650, 9.88404542e-05,
                     0.0001046496277, 6.19051218e-05, 6.47087250e-05,
                     4.57420923e-05]),
    }

#values of r0 that Cooperstock and Tieu used:
r0_ct = {'Milky Way': 35, 'NGC3031': 22, 'NGC3198': 32, 'NGC7331': 41,}

#largest radius to show on axis of plots of CT fits:
rf = {'Milky Way': 30, 'NGC3031': 22, 'NGC3198': 30, 'NGC7331': 37,}

#values of -k_n*C_n coefficients I obtained, using the data from Steven Tieu
approx = {'Milky Way':
       scipy.array([0.001263649286795494, 0.0004520162153578804,
                    0.0001785398746328821, 0.000294661842490868,
                    1.033721221021169e-05, 0.0002127639150936687,
                    -2.210211902978941e-05, 0.0001346279409514108,
                    -1.23826819184046e-05, 6.669741581606752e-05]),
      'NGC3031':
        scipy.array([0.001169410348399606, 0.0004356556833834331,
                     0.0003677376755188996, 0.0001484103796451662,
                     8.37048342824309e-05, 4.14084700629717e-05,
                     4.29270238985451e-05, 5.501307407044624e-05,
                     2.38560738746541e-05, 1.298417452452569e-05]),
      'NGC3198':
        scipy.array([0.0009317969510672148, 0.0002070296388261263,
                     0.0002259716947289554, 9.477773771099414e-05,
                     7.602079411216118e-05, 6.210099476296988e-05,
                     2.980597236442206e-05, 3.155662183064841e-05,
                     1.46059419389556e-05, 3.657978713230664e-05]),
      'NGC7331':
        scipy.array([0.00150123694318497, 0.0003027886068547498,
                     0.0003987892282241637, 0.0001838608856891028,
                     0.0002191778202465569, 9.19047571928933e-05,
                     0.0001061939549869137, 5.601236447573902e-05,
                     6.463618295809339e-05, 4.079698936264788e-05]),
```

```
    }

err = {#error bars of Cooperstock and Tieu's data
  'Milky Way':
    scipy.array([scipy.nan]*len(y['Milky Way'])),
 'NGC3031':
   scipy.array([scipy.nan]*len(y['NGC3031'])),
 'NGC3198':
   scipy.array([ 7756.8, 5870, 5031.4, 5660.4, 4192.8, 3773.6, 3564, 3144.6,
                 2096.4, 2096.4, 1886.8, 2096.4, 2096.4, 2306, 2096.4, 2306,
                 2306, 1886.8, 2096.4, 2096.4, 2096.4, 1886.8, 2096.4, 2096.4,
                 2306, 3144.6, 3144.6]),
 'NGC7331':
   scipy.array([5193, 53412, 5193, 5193, 5193, 5193, 6231.6, 6231.6, 6231.6,
                 6231.6, 4302.6, 3264, 3264, 3264, 3412.5, 3264, 3412.5, 3264,
                 3264, 3264, 3412.5, 3264, 3264, 3264, 3264, 4154.4, 4302.6,
                 5341.2, 5341.2, 5193, 7269.9, 9198.9]),
}

#the datapoints plotted in CTs paper (i.e. with several points removed)
reduced_ct = {'Milky Way': range(1,len(x['Milky Way'])),
 'NGC3031': range(len(x['NGC3031'])),
 'NGC3198': range(3,len(x['NGC3198'])),
 'NGC7331': range(1,len(x['NGC7331'])-1),
}

def loadfile(filename, comment='#!'):
    '''used for extracting rotation curve data from THINGS files'''
    f = open(filename, 'rt')
    lines = [line.split() for line in f.readlines() if line[0]
                not in comment]
    a = scipy.empty((len(lines), len(lines[0])))
    for i, line in enumerate(lines):
        for j, e in enumerate(line):
            a[i,j] = float(e)
    f.close()
    return a

def things_data(galaxyname):
    '''extracts rotation curve data from files'''
    a = scipy.loadtxt(r'C:\Documents and Settings\Cathy\My Documents\docs'\
        r'\480 project\THINGS\Curves\%s.curve.02'%galaxyname)
    y = 1000*a[:, 1]
    err = 1000*a[:, 6]
    x = loadfile(r'C:\Documents and Settings\Cathy\My Documents\docs\480 '\
        r'project\%s\data\%s.ISO.fix.REV.Kr.txt'
                    %(galaxyname, galaxyname))[:, 0]
    rf = x[-1]
    return galaxyname, x, y, err, rf,

r0opt = { #optimal r0s obtained from r0_optimiser.py (We have assigned
#the value of r0=35 to the Milky Way as we have no uncertainty data
#for this galaxy with which to calculate the optimal r0)
 'Milky Way': {4: 35, 5: 35, 6: 35, 7: 35, 8: 35, 9: 35, 10: 35},
 'NGC3031':{4: 11.584883424383 58, 5: 13.61201741490073, 6: 14.71907336455069,
            7: 17.662999001959928, 8: 23.980811816283911,
            9: 54.526120908724451, 10: 25.621672086331611,
            15: 15.449122032600766},
 'NGC3198':{4: 36.9159517288179, 5: 37.42630758623128, 6: 38.798922236058793,
            7: 37.189037676956033, 8: 38.36609642824218, 9: 38.491590416396647,
            10: 40.935789928296032, 15: 40.426542163467815},
 'NGC7331':{4: 24.40701499953861, 5: 24.90209975465989, 6: 26.088960020476119,
            7: 26.065662051690861, 8: 27.02978427827345, 9: 25.43664013308274,
```

```
            10: 26.403248621563389, 15: 26.068069450708542},
 'NGC2403':{4: 17.664001050342918, 5: 16.665404586468256,
            6: 17.079425755226936, 7: 16.82081151674717, 8: 16.93304924846943,
            9: 17.063772037496456, 10: 17.030717397141057,
            15: 18.549597842048389, 20: 18.243622018395957},
 'NGC2841':{4: 40.7678616349896, 5: 47.62649131181233, 6: 44.899400981299692,
            7: 48.759959534379064, 8: 48.792168544729549, 9: 49.41664473974491,
            10: 50.054080923630465, 15: 52.420214223852255,
            20: 54.881242758333045},
 'NGC2976':{4: 354.72890625000019, 5: 2.7966151706098268, 6: 2.9700292661099699,
            7: 2.5766894236773772,8: 2.6379293484003625, 9: 2.5495522552480301,
            10: 2.6291743896890383, 15: 2.9355110827212534},
 'NGC3521':{4: 23.277093880259265, 5: 28.174479374289518, 6: 25.584193569407574,
            7: 29.321582348865661, 8: 30.635921841755049, 9: 30.246175114686285,
            10: 30.856309478792053, 15: 74.905783081053343,
            20: 30.12758105591832},
 'NGC4736':{4: 7.2425004794262353, 5: 7.4947199859190938, 6: 7.7854900618883214,
            7: 8.1043240618911412,8: 8.6299437311788534, 9: 9.2956206341274079,
            10: 9.7285667896066492, 15: 9.2725537205735336,
            20: 9.239155136679873},
 'NGC5055':{4: 33.892853856707603, 5: 35.697603748614597, 6: 38.249162771470139,
            7: 35.523623665049676, 8: 37.020220536203126, 9: 37.980695345718374,
            10: 39.821272364724422, 15: 41.845435714721717,
            20: 42.542037200989824},
 'NGC6946':{4: 18.450361472574411, 5: 16.926762925926607, 6: 17.09710866642234,
            7: 18.083430122968068, 8: 16.610840803881494, 9: 18.280161360713343,
            10: 19.59091401869302, 15: 21.590077708164849,
            20: 19.167237823283699},
 'NGC7793':{4: 6.5255699303106649, 5: 6.9291489024413622, 6: 7.004891230165958,
            7: 6.9978439131857169,8: 7.1065023835641528, 9: 7.1312637537717825,
            10: 7.1391308553516861, 15: 7.3416768133640273},
 'NGC925':{4: 14.320267437392761, 5: 15.846348001832718, 6: 57.499521142244348,
           7: 13.649543510936198,8: 14.248294461389573, 9: 16.634974495047459,
           10: 19.576825270002978, 15: 13.591012018918992},
 'ddo154':{4: 7.7716166319150961, 5: 9.2392306566238425, 6: 10.006903468567419,
           7: 12.221991211990822, 8: 8.3569061604949599, 9: 8.425838736693068,
           10: 8.6134806836644806, 15: 9.4269916887084637},
 'ic2574':{4: 1190.8500000000372, 5: 325.7649488937808, 6: 14.253621378773824,
           7: 20.808121804303184, 8: 95.784374924004027, 9: 12.106430803925885,
           10: 11.815782088646927, 15: 12.553974936162374},
 'NGC2903':{4: 27.346362270321691, 5: 27.411453757559258, 6: 28.505385711400109,
            7: 29.747854363918311,8: 30.891289918580664, 9: 31.282965620184306,
            10: 29.052105041873311, 15: 28.723918596251515}
}

class Galaxy:
    '''assigns various properties to each galaxy'''
    def __init__(self, name, x, y, err, rf, r0opt, mkc_ct=None, r0_ct=None):
        self.name = name      #galaxy name
        self.x = x            #radii from centre of galaxy
        self.y = y            #rotation velocities at these radii
        self.rf = rf          #max radius to plot
        self.mkc_ct = mkc_ct #Cooperstock and Tieu's -k_n*C_n values
        self.r0_ct = r0_ct    #r0 used by Cooperstock and Tieu
        self.err = err        #uncertainties of rotation curve data
        self.r0opt = r0opt    #optimal value of r0 from r0_optimiser.py

galaxynames = ['Milky_Way', 'NGC3031', 'NGC3198', 'NGC7331','ddo154','ic2574',
               'NGC925', 'NGC2403', 'NGC2841', 'NGC2903', 'NGC2976','NGC3521',
               'NGC4736', 'NGC5055', 'NGC6946', 'NGC7793']

galaxies = [Galaxy(name, x[name], y[name], err[name], rf[name], r0opt[name],
                   mkc_ct[name], r0_ct[name],) for name in galaxynames[:4]]
```

```
galaxies_reduced = [Galaxy(name, x[name][reduced_ct[name]],
                    y[name][reduced_ct[name]], err[name][reduced_ct[name]],
                    rf[name], r0opt[name], mkc_ct[name], r0_ct[name],)
                    for name in galaxynames[:4]]

#initial estimates of optimal r0, used as starting values for r0_optimiser
faker0opt = {4: 25, 5: 25, 6: 25, 7: 25, 8: 25, 9: 25, 10: 25}

galaxies_things = [None]+[Galaxy(*(things_data(name) +(r0opt[name]
                          if r0opt.has_key(name) else faker0opt,
                          mkc_ct[name] if mkc_ct.has_key(name) else None,
                          r0_ct[name] if r0_ct.has_key(name) else None,)))
                          for name in galaxynames[1:]]

def thingsMONDdata(galaxyname):
    '''loads data to create MOND fits'''
    data = loadfile(r'C:\Documents_and_Settings\Cathy\My_Documents\docs'\
        r'\480_project\%s\data\%s.ISO.fix.REV.txt'%(galaxyname, galaxyname))
    vobs = 1000*data[:, 4]    #observed rotation velocity
    err = 1000*data[:, 5]     #uncertainties of rotation curve data
    r = data[:, 0]            #radii from centre of galaxy
    vgas = 1000*data[:, 1]    #rotation velocities of gas in the galaxy
    vdisk = 1000*data[:, 2]   #rotation velocities of the galactic disk
    vbulge = 1000*data[:, 3] #rotation velocities of the central bulge
    rf = r[-1]                #outermost radius to plot
    return galaxyname, r, vobs, err, vgas, vdisk, vbulge, rf

class GalaxyMOND:
    def __init__(self, name, r, vobs, err, vgas, vdisk, vbulge, rf):
        self.name = name
        self.r = r
        self.vobs = vobs
        self.rf = rf
        self.err = err
        self.vgas = vgas
        self.vdisk = vdisk
        self.vbulge = vbulge

galaxiesMOND = [None]+[GalaxyMOND(*thingsMONDdata(name))
                       for name in galaxynames[1:]]
```

r0_optimizer.py

```
import scipy
import data
import pylab
import bessel_plotter
import pprint

def galaxyr0s(galaxies, parameters):
    '''calculates the optimal value of  r0 for all galaxies'''
    r0opt = {}
    for galaxy in galaxies:
        print galaxy.name
        r0opt[galaxy.name] = {}
        for constraint in parameters:
            minim = bessel_plotter.r0min(galaxy, constraint)
            r0opt[galaxy.name][constraint] = minim[0]
    return r0opt

if __name__ == '__main__':
    r0opt = galaxyr0s(data.galaxies_things[1:15], range(10, 11))
```

```
    pprint.pprint(r0opt)
#     galaxy = data.galaxies_things[5]
#     r0s = scipy.linspace(1, 80, 200)
#     c=10
#     pylab.semilogy(r0s, [bessel_plotter.chi2err(r0, galaxy, c)
#                          for r0 in r0s])
#     minim = bessel_plotter.r0min(galaxy, c)
#     pylab.plot(minim[0], [minim[1]], 'r+', markersize=10)
#     pylab.title(galaxy.name+' chi^2 vs r0')
#     pylab.show()

#The above commented text would plot the chi^2 vs r0 to check that
#the optimal r0 obtained did in fact give the global minimum chi^2.
```